Published in final edited form as:

FASEB J. 2021 February ; 35(2): e21327. doi:10.1096/fj.202002323R.

Physiological Effects of Inactivation and the Roles of *Elovl3*/ ELOVL3 in Maintaining Ocular Homeostasis

Amber Wilkerson[*], **Nita Bhat**[*,a], **Hoang Quoc Hai Pham**[*,b], **Seher Yuksel**[*], **Igor Butovich**[*,†,#]

[*]Department of Ophthalmology, University of Texas Southwestern Medical Center, Dallas, Texas, USA

[†]The Graduate School of Biomedical Sciences, University of Texas Southwestern Medical Center, Dallas, Texas, USA

Abstract

Recently, elongase of very long chain fatty acids-3 (ELOVL3) was demonstrated to play a pivotal role in physiology and biochemistry of the ocular surface by maintaining a proper balance in the lipid composition of meibum. The goal of this study was to further investigate the effects of ELOVL3 ablation in homozygous *Elovl3*-knockout mice (*E3hom*) in comparison with age and sex matched wild type controls (*E3wt*). Slit lamp examination of the ocular surface of mice, and histological examination of their ocular tissues, highlighted a severe negative impact of *Elovl3* inactivating mutation on the Meibomian glands (MG) and conjunctiva of mice. MG transcriptomes of the *E3hom* and *E3wt* mice were assessed and revealed a range of up- and down-regulated genes related to lipid biosynthesis, inflammation and stress response, compared with *E3wt* mice. Heat stage polarized light microscopy was used to assess melting characteristics of normal and abnormal meibum: The loss of *Elovl3* led to a 8°C drop in the melting temperature of meibum in *E3hom* mice, and increased its fluidity. Also noted were the excessive accumulation of lipid material and tears around the eye and severe ocular inflammation, among other abnormalities.

Keywords

Meibomian glands; meibum; transcriptomics; *Elovl3*; elongase of very long chain fatty acids; meibogenesis; lipid homeostasis

[#]**Correspondence**: Dr. Igor A. Butovich, Department of Ophthalmology, University of Texas Southwestern Medical Center, 5323 Harry Hines Blvd., Dallas, TX 75390-9057, USA, igor.butovich@utsouthwestern.edu.

[a]Present address: Department of Internal Medicine, Howard University Hospital, Washington, DC, USA

[b]Present address: Irell & Manella Graduate School of Biological Sciences, Beckman Research Institute, City of Hope National Medical Center, Duarte, CA, USA

AUTHOR CONTRIBUTIONS

I. A. Butovich designed the project, planned and performed transcriptomic and lipidomic experiments, analyzed data, and wrote the manuscript. A. Wilkerson wrote the manuscript, obtained mouse ocular samples and performed their histological characterization. N. Bhat participated in histological and thermotropic characterization of the samples and data analyses. H. Pham participated in thermotropic characterization of the mouse tissue samples and data analysis. S. Yuksel participated in lipidomic experiments and data analysis. All co-authors discussed the data, edited the manuscript, and reviewed its final version.

INTRODUCTION

The holocrine Meibomian glands (MG) reside within the tarsal plates (TP) of the eyelids of humans and most of other mammals and secrete an oily substance called meibum (1). The chemical analyses of meibum revealed that it is composed predominantly of lipids with up to 20% of non-lipid inclusions (2). Meibum lipids are believed to form the outermost layer of the tear film (TF), called TF lipid layer (TFLL) that covers the entire ocular surface (3, 4). Meibum is an extremely complex secretion that is comprised of both polar and nonpolar lipids including families of wax esters (WE), cholesteryl esters (CE), free fatty acids (FFA), triacylglycerols (TAG), (*O*)-acylated ω-hydroxy fatty acids (OAHFA), cholesteryl esters of OAHFA (Chl-OAHFA), and diacylated α,ω-diols (DiAD), as well as free cholesterol (Chl), squalene, and a range of phospholipids, sphingomyelins, and, possibly, other minor lipid components. The non-lipid components of meibum include proteins (5–7), most likely in various degrees of unfolding and/or hydrolysis, fragments of DNA/RNA, and, with all likelihood, water and minerals.

It has been demonstrated that TF in general, and TFLL specifically, play vital roles in physiology of the ocular surface: They protect the eye from desiccation (8), lubricate cornea and conjunctiva (9), may prevent ocular surface infections (10), and help to maintain visual acuity (11, 12). It is plausible that alterations in TP/MG homeostasis can be detrimental for ocular health, and, in severe cases, may lead to various multifactorial ocular pathologies such as blepharitis, dry eye disease and chalazia. Note that blepharitis is often associated with bacterial infections (13, 14). Thus, adverse changes in meibum composition may affect the ability of TF/TFLL to maintain their structural integrity and interact with other elements that promote a healthy ocular surface.

In order to understand how MG function, animal models with targeted inactivating mutations in genes involved in meibogenesis have been proposed and studied (15–18). It was demonstrated that selective inactivation of those genes led to dramatic changes in MG morphology and ocular surface physiology, and severely abnormal meibomian lipid profiles. Of those genes, the elongase of very long chain fatty acids 3 (ELOVL3) is important because the enzyme functions as a rate-limiting step and a pivotal point in the fatty acid elongation cycle elimination of which leads to termination of the biosynthesis of saturated FA longer than C_{20}, and completely transforms lipid profile of meibum (16). The purpose of this study was to further investigate the physiological consequences of the loss of *Elovl3*/ELOVL3, analyze the thermotropic characteristics of mutant meibum, and conduct comparative transcriptomic studies of TP of wild-type and *Elovl3*/ELOVL3-ablated mice.

MATERIALS AND METHODS

Reagents

Authentic lipid standards were obtained from Nu-Check Prep (Elysian, MN, USA) and MilliporeSigma (St. Louis, MO, USA). Analytical grade salts, acids, and bases were from MilliporeSigma and ThermoFisher Scientific (Waltham, MA, USA). Ultra-high performance chromatography (UPLC) and mass spectrometry (MS) grade solvents were from Honeywell

Burdick & Jackson and Fisher Chemical (both purchased from ThermoFisher Scientific), and MilliporeSigma.

Animals

All procedure that involved live animal were conducted in accordance with the Association for Research in Vision and Ophthalmology (ARVO) Statement for the Use of Animals in Ophthalmic and Vision Research. All animal procedures were approved by the Institutional Animal Care and Use Committee of the University of Texas Southwestern Medical Center.

The *Elovl3*^{burf}/GrsrJ founder mutant mice (stock no. 024182) were obtained from The Jackson Laboratory (Bar Harbor, ME, USA). Animals were characterized and genotyped as previously described (16) using the same primers. Age and sex matched mice with expunged *Scad* mutation were used for these studies. The ages of mice depended on the type of the experiments and are indicated further in the text or in the figure legends. All mice were housed in ventilated microisolator cages on a 12-h light/dark cycle with free access to food (a Teklad 2016 16% Protein rodent diet; from Envigo, Indianapolis, IN) and water.

Ocular evaluation

Mice were lightly anesthetized with xylazine/ketamine cocktail and their ocular surfaces were examined by a slit lamp (model BQ 900 from Haag-Streit USA, Inc. Mason, OH, USA). Images were taken using an interfaced Canon EOS Rebel T6i digital camera (Canon, Melville, NY, USA).

Histology and Immunohistochemistry

Animals were euthanized, tissues were collected under a Zeiss Stemi 508 Stereo microscope (Carl Zeiss, Oberkochen, Germany), and treated as described before (16). Briefly, the specimens were placed in buffered Carson's formalin for more than 24 hours. Then, the tissues were dehydrated in serial dilutions of ethanol, cleared in xylene for 1 hr and embedded into paraffin blocks. Tissue sections were cut at 4μm using a Leica CM3050S cryostat (from Leica Biosystems Inc., Buffalo Grove, IL, USA) and consequently stained with hematoxylin and eosin (Statlab, McKinney, TX, USA). The tissue slides were studied using bright field microscopy using a Zeiss Observer D1 microscope and the Axiovision software (also from Carl Zeiss).

Transcriptomic Analysis of Mouse Tarsal Plates

Mouse TP collected from six *E3wt* and six *E3hom* age-matched animals (equally males and females) were used for transcriptomic analysis. TP were excised from freshly euthanized mice as described before (16, 19), placed in RNAlater reagent (Quiagen, Germantown, MD, USA) and stored at −20°C until the mRNA was forwarded to the UTSW Genomic and Microarray Core Facility for RNA extraction and analysis. The integrity of extracted mRNA was checked prior to transcriptomic analysis. Only samples with RNA integrity numbers above 9 were used in the study. Specimens were analyzed using Clariom D microarrays (Affymetrix, Santa Clara, CA, USA). The RNA expression data were processed in the Expression Console software package (v.1.4.1.36 from Affymetrix) and Transcriptome Analysis Console (v.4.0.1, TAC; from the same manufacturer). The data were statistically

analyzed using the TAC build-in statistical routines and SigmaStat package v.3.5 (from Systat Software Inc., Point Richmond, CA). A non-parametric empirical Bayes Anova (eBayes) method (a part of the TAC software package) was used to rank differentially expressed genes. Based on industry-standard settings, the linear fold changes (LFC) in gene expression patterns (GEP) that satisfied the following criteria – $(-2) \geq LFC \geq (+2)$ and $p \leq 0.05$ – were considered statistically significant. The gene enrichment and pathways analyses were performed in TAC and IMPaLA (available through http://impala.molgen.mpg.de).

Liquid Chromatography/Mass Spectrometry of Lipids

A Waters Synapt G2-Si high resolution quadrupole Time-of-Flight (qToF) mass spectrometer equipped with IonSabre-II atmospheric pressure chemical ionization (APCI) ion source and a LockSpray unit were used (all from Waters Corp., Milford, MA, USA). Chromatographic separation of the analytes was achieved on a Waters M-Class UPLC system using an Acquity UPLC C_{18} BEH column (1 mm×100 mm, 1.7 μm; also from Waters). Raw UPLC/MS and MS^E files were analyzed in Waters MassLynx (v.4.1) and MS^E DataViewer (v.1.4) software packages and the elemental CHNO compositions of lipids were computed using the MassLynx EleComp (v.4.0) as described earlier (19–21).

A reversed phase (RP) UPLC/MS protocol that had been used in a preceding publication (16) was precisely followed. Pooling of samples from different mice was unnecessary as the sensitivity of the instrumentation was adequate to work with individual TP. WE, CE, and TAG standards were analyzed alongside meibomian lipid samples for comparison purposes in targeted supervised experiments. The meibum lipid samples were also compared using untargeted, unsupervised approach which was based on the Principal Component Analysis (PCA) of the raw UPLC/MS data using Progenesis QI software package (from Waters).

Hot Stage Cross-Polarized Light Microscopy

Hot stage cross-polarized light microscopy (HSPLM) evaluation of samples was performed using a Nikon Eclipse 50i POL microscope (from Nikon Instruments, Melville, NY) and an LTS420 heating-cooling stage (from Linkam Scientific Instruments, Waterfield, UK). A Nikon DS-Fi1 color digital camera integrated with the microscope was used for recording the data. The results were analyzed in NIS-Elements BR software package (from Nikon).

Freshly excised TP specimens were placed in 4% paraformaldehyde in phosphate buffered saline overnight, then run through a serial dilution of sucrose in phosphate-buffered saline from 10% to 30% and placed in 30% sucrose overnight. The following day TP were placed in the optimal cutting temperature compound (OCT) blocks and stored at −80 °C. Tissue sections were cut 10μm thick and placed on chilled glass slides. Prepared tissue slides were stored at −80 °C until further use. Microscopic evaluation of the TP tissue was performed using the Nikon HSPLM system and the heating/cooling cryostage as described before (5).

RESULTS

Evaluation of the Ocular Phenotype

Under slit lamp examination, the TF of *E3hom* mice appeared to be thicker than the TF of *E3wt* mice, which had normal appearance (Figure 1, Panels A, B). The TF of mutant mice was populated with oil-like droplets clearly visible on the lower part of the cornea (Figure 1, Panel C). The *E3hom* mice had varying degrees of crusty deposits around the eye opening and puffy eyelids with hair and lash loss. The mice had difficulty to keep their eyes open: The thick crust kept the eyes tightly shut for varying periods of time before they could re-open (Figure 1, Panel D). Generally, *E3hom* mice had a slit-eye phenotype which persisted with aging. The eyelid margin of *E3hom* mice had enlarged MG orifices surrounded by dilated blood vessels (Figure 3, Panel E). The tears excessively accumulated on the cornea and at the eyelid margins of *E3hom* mice and easily overflew onto the proximal eyelid skin. By 12 month old, the *E3hom* mice had excessive conjunctival folds resembling those of human conjunctivochalasis, which were not observed for wild-type mice (Figure 1, Panels F and G). Also, the previously reported neovascularization of the cornea of *E3hom* mice (16) was observed in this study as well (Figure 1, Panel G).

E3wt and *E3hom* TP specimens underwent gross evaluation at removal. When excising the TP in *E3hom* mice, special care had to be taken to avoid loss of meibum: The slightest pressure exerted on the eyelid resulted in expression of clear liquefied MG secretions from the MG orifices that quickly spread onto the surrounding tissues. The TPs were excised from upper and lower eyelids and placed on chilled glass dissection plate where superfluous tissues (conjunctiva and muscle) were removed, prior to being placed into the RNAlater solution or fixative. Note that while trimming tissue from the TP of *E3hom* mice, some meibum could be lost due to its high fluidity and accumulated on the dissecting plate. Therefore, chilling the samples during all procedures was necessary.

E3hom mice were prone to development of eyelid ulcerations (Figure 2, Panel A). Despite the heavily ulcerated and disfigured eyelids, the MGs retained their normal shape with clearly visible central ducts with accumulated meibum (Figure 2, Panel B). However, upper and lower TPs of *E3wt* had equally spaced acini with barely discernible vessels (Figure 2, Panels C, D), while the *E3hom* MGs acini were converging and becoming progressively narrower towards the orifice with a large MG of the lateral canthus that seemed to protrude beyond the normal region and encased the blood vessel that fed into the eyelid (Figure 2, Panels E, F). The central ducts of several *E3hom* mice had a noticeably greenish hue with highly visible dilated blood vessels (not shown). In 1-yr old *E3hom* mice, the MGs in the lower eyelid were narrow at the eyelid margin and widened towards the beginning of the central duct (Figure 2, Panel G). Neither *E3wt* nor *E3hom* mice manifested MG dropout at any age, unless it was a *E3hom* mouse with a severely ulcerated eyelid.

Histological evaluation of the TPs revealed noticeable abnormalities in MGs caused by *Elovl3* inactivation. *E3wt* mice displayed typical meibocyte maturation and rupture patterns with sporadically observed mitotic cells. The surrounding tissue, hair follicles, and conjunctiva lacked any signs of inflammation in 2 to 18 months old *E3wt* mice (Figure 3, Panel A1–A3). Conversely, the *E3hom* acini had visible signs of inflammation with

numerous mitotic cells within the acini and ductal epithelium even in 3.5 months old animals (Figure 3, Panels B1-B3) with a tendency to worsen with aging.

At the same time, *E3wt* mice demonstrated no noticeable age-related pathologies in their MG and adnexa (Figure 4, Panels A–C). When moving from ascini to central ducts, *E3wt* meibocytes underwent typical maturation, rupture, and complete disintegration, resulting the release of meibum at the acinus to ductile transition. No ductile or central duct plugging was observed. On the other hand, the MG, conjunctiva and hair follicles of the eyelids of aging *E3hom* mice were abnormal (Figure 4, Panels D–H). The *E3hom* ductal epithelium was thick and populated with abnormal nuclei, nuclear remnants, inflammatory cells, and accumulation of cellular debris within the central duct, which were not observed in *E3wt* mice. The *E3hom* acini were numerous and basophilic. By the age of 15 months, the *E3hom* mice developed severe chalazion-like lipogranulomatous inflammation, and acinar loss (Figure 4, Panel F–G). The orifices were dilated with large accumulations of the incompletely disintegrated meibocytes (Figure 4, Panel H).

Thermotropic characteristics of *E3wt* and *E3hom* meibum.

We previously reported that inactivation of *Elovl3* gene led to an increase in short chain and unsaturated fatty acids in meibum (16). Thus, we hypothesized that melting temperature of *E3hom* meibum would be considerably lower than that of *E3wt* mice. To test this hypothesis, melting characteristics of *E3wt* and *E3hom* mouse meibum that was still embedded in the surgically excised TP were studied using HSPLM exactly as described in our earlier publication for wild type mice (5). The method utilizes the well known birefringent properties of lipids and lipid mixtures, such as meibum, which originate from their ability to form liquid crystals and self-organize into ordered supramolecular structures (membranes, lamellas, micelles, etc.). This ability of lipids is essential for differentiating lipids from amorphous non-melting materials like proteins. Representative microphotographs of the changes in birefringence of a TP tissue sample upon heating are shown in Figure 5, Panels A, B, and C. At low temperatures, initially solid crystal- or liquid crystal-like meibum is visible as bright (birefringent) structures on a dark (non-birefringent) background. However, upon heating, meibum melts and (liquid) crystals disintegrate to form disorganized pools of lipid with no birefringent properties which blend with the background. Note that repetitive heating/cooling cycles were possible with *E3wt* mouse meibum but not with *E3hom* one because of a much higher fluidity of the latter: After the first heating cycle, a large portion of meibum escaped its natural reservoir in MG and spread to form a very thin layer which lost all birefringence features due to its thinness.

When the intensity (or brightness) of birefringence of meibum was plotted against the sample's temperature and the experimental data were approximated using a cubic spline curve fitting technique (Figure 5, Panel D), a clear evidence of a dramatic effect of the *Elovl3* inactivating mutation on the melting characteristics of meibum was obtained: The *E3hom* meibum started to melt at well below 0 °C and was almost completely liquefied at about 39 °C, which is slightly over the physiological mouse ocular surface temperature of ~37 °C (22). The *E3wt* meibum, on the other hand, did not start to melt until well above 10 °C, and became completely liquefied only at 49–50 °C. In a physiologically important range

of temperatures between 30 °C and 40 °C, *E3wt* meibum remained in a highly to partially organized liquid-crystal state, while *E3hom* meibum was almost completely melted.

To quantitate these changes, the spline curves were numerically differentiated to find inflection points on the melting curves (Figure 5, Panel E). Indeed, there were two inflection points found for each curve, T_1 = (272±2) K and T_2 = (298±1) K for *E3hom* meibum, and T_1 = (289±2) K and T_2 = (307±1) K for *E3wt* meibum (n=3 for each group). These inflection points denote the temperatures at which the fastest changes in the melting of samples occur. Note that the spline curve fitting technique does not depend on any specific biological, chemical, or physical model or mechanism. Thus, the results of calculations were unbiased and could be used as starting points for further theoretical analysis of the data.

The first consideration was a clearly non-linear, cooperative character of meibum melting. Secondly, in accordance with our previous results (5), meibum melting produced two inflection (or transition) points, T_1 and T_2. A simplest mechanism that describes such behavior is as follows:

$$\text{Crystal (solid, birefringent)}$$

$$\text{Partially melted (liquid crystal, birefringent) } (T_1)$$

$$\text{Partially melted (liquid crystal, birefringent) } (T_2)$$

$$\text{Melted (liquid, non-birefringent)}$$

Thus, a three-phase, two transition temperatures cooperative Hill-type Equation 1 was used:

$$I_{br} = A - \left(B \times T^k\right)/\left(T_1^k + T^k\right) - \left(C \times T^m\right)/\left(T_2^m + T^m\right) \quad (1)$$

where I_{br} is current birefringence, A is initial (i.e. highest) birefringence of fully solidified meibum (which equals 1, if normalization is used), B and C are relative contributions of the two other birefringent forms of meibum to the resulting melting curve (both are greater than zero, but less than 1), T is the current temperature of the sample (in K), T_1 and T_2 are two phase transition temperatures, while k and m are the Hill cooperativity coefficients (unitless). The parameters of Eq.1 were found using Equation 1 and a nonlinear curve fitting routine (Table 1). The resulting curves are presented in Figure 5, Panel F showing an excellent fit. Note a considerable drop in the Hill cooperativity coefficients k and m and transition temperatures T_1 and T_2 for *E3hom* mice that reflected dramatic changes in the thermotropic characteristics of meibum caused by the mutation.

Calculations were repeated for three samples of each kind and showed only moderate variability in the data: transition temperatures T_1 and T_2 were found to be virtually identical to those calculated using the spline approximation approach (see above) with SD of ±2.3°C,

while parameters ***B***, ***C***, ***k*** and ***m*** varied within ±16%, making differences between *E3wt* and *E3hom* statistically significant ($p < 0.05$) for both cooperativity coefficients ***k*** and ***m***, but not for ***B*** and ***C*** ($p<0.2$). The strict interpretation of physicochemical meaning of these parameters goes beyond the scope of this manuscript and is to be addresses in future studies. However, the generalized trend of lowering transition temperatures T_1 and T_2 and reduction in cooperativity of melting as results of *Elovl3* inactivation have far reaching physiological consequences that are discussed later in the paper.

Untargeted transcriptomic evaluation of *E3wt* and *E3hom* tarsal plates

Inactivation of *Elovl3* caused a landslide shift in the lipid profiles of meibum which were evaluated in details in our recent paper (16). Also, the mutation dramatically impacted ocular physiology of mice in general. Though the causes and molecular mechanisms of those effects are complex and remain largely unknown, it is reasonable to hypothesize that inactivation of a critically important gene (such as *Elovl3*) may trigger changes up- and downstream of its place in meibogenesis, and may also affect other biosynthetic and regulatory pathways in MG. To test these hypotheses, we conducted comparative transcriptomic analysis of *E3hom* and *E3wt* mouse TP specimens using mRNA microarrays as described earlier for wild-type mice (7, 20).

The following observations were made. Of 65,956 transcripts detected in microarray experiments, 3,251 (or 4.93%) genes passed the criteria of $(-2) \geq \text{LFC} \geq (+2)$ and $p \leq 0.05$ (Figure 6). Thus, they were considered to be differentially expressed. Of those, 387 protein-coding genes were increased, while 392 – decreased as a result of the mutation. The pool of pseudo-genes was also affected, and so where other transcripts (Table 2):

Then, a list of differentially expressed protein-coding genes with known functions was compiled using the TAC software and mRNA microarray gene expression datasets for *E3hom* and *E3wt* mice. The genes for which LFC were either ≤ -2, or ≥ 2, and *p*-values were ≤ 0.05 (about 1,200 in total), were selected and their compilation was analyzed using IMPaLA (Integrated Molecular Pathway Level Analysis) online tool using its “Pathway Over-Representation Analysis” and “Wilcoxon Pathway Enrichment Analysis” routines. A list of 200 most over-represented pathways can be found in Suppl. Table 1. Characteristically, the pathways related to biosynthesis, functions, and degradation of lipids, cholesterol, and fatty acids were on top of the list representing at least 87 out of 200 identified pathways. Also significant were pathways related to muscle contraction and biosynthesis and metabolism of keratin, among other processes. Finally, genes related to inflammation were analyzed as well). For evaluation of the inflammation-related genes, online databases, such as IMPaLA, GeneCards, Brenda, and UniProt were searched and a list of genes was assembled (see below). Surprisingly, they were not among top ranked differentially expressed genes in mutant mice as their pathways ranked low with P_{genes} and Q_{genes} values of ≥ 0.125 and ≥ 1, respectively. Such a low significance indicated that inflammatory processes in *E3hom* MG themselves were much more subdued then those in adnexa.

The Wilcoxon Pathway Enrichment Analysis (Suppl. Table 2) produced just three pathways that had both P_{genes} and Q_{genes} values better than 0.05 (“Muscle Contraction”, “Lipid

Metabolism", and "Striated Muscle Contraction" pathways), with others largely duplicating pathways listed in Suppl. Table 1.

Targeted transcriptomic and lipidomic analyses of *E3wt* and *E3hom* tarsal plates.

For further, more targeted, analyses, pathways that had the lowest P_{genes} and Q_{genes} values *and* were related to lipid metabolism were selected. Because genes that were included in the "Metabolism of Lipids" pathway (Suppl. Tables 1 and 2) only partially overlapped with our list of 50 top genes of meibogenesis (16, 23), both sources were used for more focused analyses of the samples (see next section). The changes in the GEP revealed that the *Elovl3* inactivating mutation affected the mRNA levels of a range of genes related specifically to *meibogenesis*. As meibogenesis results in production of several distinctively different classes of lipids (19, 24), its major biosynthetic cores were investigated as follows.

As a first step, meibomian lipidomes were subjected to reverse phase UPLC and APCI MS analyses, followed by unsupervised PCA of the raw UPLC/MS data files. A summary bi-plot graph of the results of unsupervised PCA analyses of *E3hom* and wild type lipidomes is shown in Figure 7. Each genotype produced one group of samples each of which co-localized with specific groups of lipids: *E3hom* specimens were strongly associated with shorter-chain CE, while their wild-type counterparts – with longer-chain WE and CE. Thus, these groups of lipids, and their related genes, were evaluated in more depth.

Biosynthesis of cholesterol and cholesteryl esters.—The most up-regulated gene of all was *Idi2* (isopentenyl-diphosphate delta isomerase 2), whose mRNA level rose 271 times (($p = 2.48\times10^{-8}$). An *Idi2*'s ortholog is a pseudogene *Gm9745*, whose level was also considerably up-regulated and exceeded the norm by a factor of 230 ($p = 2.08\times10^{-8}$). IDI2 is one of the key upstream enzymes of cholesterol, squalene, and isoprenoid biosynthetic pathways that catalyzes isomerization of isopentenyl diphosphate (IPP) into its isomer dimethylallyl diphosphate (DMAPP). The latter is a precursor for prenyl diphosphates (such as geranyl, farnesyl and geranylgeranyl diphosphates) which are further metabolized into a large number of other compounds. Biosynthetically related to these functions of *Idi2* are genes shown in Table 3. Importantly, the vast majority of these genes were upregulated in MG of *E3hom* mice. However, a pair of genes *Soat1* and *Soat2* that are controlling biosynthesis of CE from free Chl and acyl-CoA, were not significantly impacted and showed barely detectable increase in LFC of, correspondingly, 1.6 ($p = 0.005$) and 1.2 ($p = 0.29$). On the contrary, gene *Lipa* that encodes a lipase with cholesteryl ester hydrolase activity was somewhat down-regulated (LFC = −2.2; $p = 3.39\times10^{-5}$).

Fatty acid elongation.—A representative MS spectrum of *E3wt* and *E3hom* TP lipids is shown in Figure 8, Panels A and B. A characteristic feature of meibum is its high enrichment with lipids based on very, extremely, and ultra long chain (VLC, ELC, and ULC, correspondingly) fatty acids and alcohols of the C_{20} to C_{34} range (1, 25). This requires a concerted work of a large number of enzymes that elongate trivial products of lipogenesis – fatty acids of the $\leq C_{20}$ chain length, – and those of dietary nature. The main enzymes that are involved in elongation of regular FA into VL, ELC, and ULC ones in mice and humans include a family of FA elongases (ELOVL1 through 7), trans-2,3-enoyl-CoA reductase

(TECR), a group of 2-hydroxyacyl-CoA dehydratases (HACD1 through 4), and a multifunctional enzyme ketoacyl-CoA reductase (KAR), also known as hydroxysteroid (17-beta) dehydrogenase 10 (HSD17B10) (26, 27), as well as a number of other genes and enzymes, some of which are listed in Table 4. While analyzing GEP of *E3hom* mice, noted was significant up-regulation of many genes of FA elongation, such as *Acat2*, *Acsbg1*, *Acat3*, *Tecr*, *Hacl1*, and *Hacd3*, but not *Elovl*s: The only *Elovl* that almost reached the threshold level of LFC of 2 was *Elovl1* (LFC = +1.8) which encodes an enzyme ELOVL1 of FA elongation cycle acting immediately down-stream of ELOVL3 (15, 16). Another member of the *Elovl* family – *Elovl7* – was significantly down-regulated (LFC = −2.4), and so were two genes of the FA elongation core *Hacd1* (−2.0) and *Hacd4* (LFC = −1.9).

The effect of *Elovl3* inactivation was most visible when analyzing meibomian CE (Figures 7 and 8, Panels C and D): A shift toward short chain and unsaturated compounds, and down-regulation of long chain *saturated* CE were in line with lower melting point of *E3hom* meibum (Figure 5). Importantly, several saturated CE of meibum were found to be branched (28). The effect of desaturation and branching on thermotropic characteristics of meibum will be briefly discussed later in the text, while a more detailed report will be published separately.

Fatty acid desaturation.—Meibum is a complex, and highly conservative in the norm (20, 23) mixture of saturated and unsaturated lipids (Figure 8, Panels A and B), maintaining the balance of which is critically important for ocular physiology as changes in the degree of unsaturation adversely affect melting characteristics of lipids. Main enzymes that control the degree of unsaturation of VLC, ELC, and ULC lipids are fatty acid desaturases (FAD) and stearoyl CA desaturases (SCD). Each enzyme family has several members that differ in substrate and product specificities, as well as their levels of expression in TP. In *E3hom* mice, only two desaturases – *Fads6* and *Scd2* – were upregulated, while just one – *Scd4* – was marginally down-regulated (Table 5). Transcription levels of other genes remained virtually unchanged. Note that log2 expression values of all genes of the *Scd* family were above 18 (20), while all *Fads* were much lower at ≤ 8.2 (current paper).

Biosynthesis of fatty alcohols.—As WE is a major class of lipids in meibum, MG needs to reduce fatty acyls to produce fatty alcohols (FAl) and achieves that by using fatty acyl CoA reductases (FAR). Two main FAR are currently known: FAR1 and FAR2. The former enzyme reportedly reduces saturated and monounsaturated C_{16} and C_{18} FA to FAl, while FAR2 – saturated ones (29). Both genes were somewhat upregulated in *E3hom* mice, but only *Far1* reached a statistically significant level of p=0.0001 and LFC=2.45, while *Far2* lagged at LFC=1.23 and p=0.131.

Fatty acid and fatty alcohol branching.—A large proportion of meibomian lipids is branched (1, 30). Branched are many WE (30) and CE (28), and, possibly, other compounds. Generally, FA and FAl branching, especially of *anteiso*-type, affects thermotropic characteristics of the isomeric compounds by lowering their melting temperatures compared with their straight-chain isomers (31–33).

Several genes and enzymes are involved in FA branching (Table 6). Interestingly, some of those genes were upregulated in TP of *E3hom* mice, including *Bckdhb*, *Pcca*, *Acox2*, and *Dbt.* This correlated well with apparent upregulation of the biosynthesis of short chain CE, such as C_{14}-CE through $C_{20:0}$-CE (Figure 8, Panels C and D), which are predominantly branched (28). Expression of other genes was affected to a much lesser extent, if at all, never reaching a statistically significant level.

Omega-oxidation of fatty acids.—Based on lipidomic data, ω-oxidation of ELC and ULC FA is essential for the normal course of meibogenesis as it leads to biosynthesis of complex esters and diesters of the OAHFA, Chl-OAHFA and DiAD families. We proposed that genes that are responsible for this transformation belong to the *Cyp/Cyp4* family (19, 24), specifically *CYP4F22* (23). Recently, Miyamoto et al. (17) demonstrated that inactivation of a mouse ortholog of this human gene – *Cyp4F39* – inhibited ω-hydroxylation of ELC/ULC FA in TP of mutant mice, confirming our predictions of its role in meibogenesis. Inactivation of *Elovl3* led to a statistically significant increase in the level of expression of *Cyp4F39* in *E3hom* mice (LFC=2.83; p=2.53E-05), implying a possible link between the two genes/enzymes.

Ocular abnormalities in *E3hom* mice.—As eyes and adnexa of *E3hom* mice routinely showed signs of inflammation, genes that are involved in inflammatory processes in TP were evaluated. First, a list of candidate genes, selected from (34, 35) and various online database, such as GeneCards, Brenda, IMPaLA, and UniProt, was assembled. Then, the expression levels of these genes in TP of *E3hom* and *E3wt* mice were determined using the TAC software and mRNA microarray gene expression datasets for *E3hom* and *E3wt* mice (Table 7). The most overexpressed genes in *E3hom* mice were vanin-1 (*Vnn1*), interferon gamma inducible protein 30 (*Ifi30*, LFC = 3.1)), and *Cd68* antigen, while the most suppressed gene were *Ifi204* (LFC = −33.0) and *Skint3* (LFC = −266.6).

DISCUSSION

Elovl3 inactivation and ocular surface homeostasis.

Our experiments demonstrated that the loss of *Elovl3* had a detrimental effect on the ocular surface causing excessive tearing, swollen eyelids, lash loss, inflammation, and corneal vascularization. We speculate that the biochemical changes in the *E3hom* meibum may have resulted in its easier expressibility due to the increased fluidity of meibum, its visibly larger quantities in MGs, and their overall larger sizes. The demand for meibogenesis may be increased as meibum is excessively secreted from the orifices quickly emptying central ducts, pools on the ocular surface and eventually overflows the eyelid margin to accumulate around the eyes. This hypothesis is supported by the observation of the increased turnover of meibocytes, the increased mitotic activity in both the duct and the acini, and the premature maturation of the meibocytes in the ductiles, which led to incomplete degradation of the meibocytes in the central duct. The increase in abnormal non-lipid inclusions (most likely, remnants of ruptured meibocytes) in the connecting ducts and the central duct could be one of many causes of their inflammation and plugging often seen in the *E3hom* mice. This hypothesis is supported by a recent study by Reneker et al. (36) who found that irregular

differentiation and epithelial hyper-proliferation can lead to MG obstruction in humans, and by our earlier observations on non-lipid proteinaceous inclusions in meibum of human MGD patients (5). On the other hand, apparent narrowing of central ducts at the MG orifices might be a result of higher fluidity of abnormal *E3hom* meibum as the less viscous secretion would not stagnate in the ductiles and ducts of MGs, and would excrete easier than meibum of wild type mice which is quasi-solid at physiological temperatures (Figure 5). Also, liquefied meibum in MG central ducts of *E3hom* mice might be less contrasty than *E3wt* meibum visually changing its appearance in the conditions of bright field microscopy.

Frequent and severe ulceration of the conjunctiva and adnexa (such as eyelid skin) of *E3hom* mice (Figure 2, Panel A) may have the same origin as skin lesions in human subjects with atopic dermatitis (37). In that study, Berdyshev et al. reported that lowering the expression levels of *Elovl3* and *Elovl6* led to an increase in short chain ceramides, sphingolipids and lysophospholipids, and a decrease in their longer-chain variants, in lesional stratum corneum. The in vivo effect was reproduced using differentiated human keratinocytes and down-regulation of ELOVL3/ELOVL6 expression by siRNA. These defects undoubtedly affected the skin barrier as it relies on very- and extremely long chain ceramides to function (38). The skin and conjunctiva ulcerations in *E3hom* mice may also be related to a severely down-regulated *Skint3*: In our hands, its levels dropped considerably in response to the mutation (LFC = − 266.6). Recently, Keyes et al. discovered that skin of the mice with conditionally knocked down *Skint3* and *Skint9* genes lacked wound-repairing ability, possibly through STAT3 pathway (39).

Interestingly, inflammatory processes in MG seemed to be relatively subdued, compared to the adnexa. One of the proteins that are overexpressed in *E3hom* TP – vanin-1, encoded by *Vnn1* – has been shown to have pro-inflammatory activity in mouse psoriatic epidermis mice (40). Vanin-1 was also characterized as an epithelial sensor of stress which controls mouse innate immune response (41). Thus, it's overexpression in *E3hom* TP might be reflecting the inflammatory processes in the affected tissues. Another gene, *Ifi204* (an ortholog of a human gene *IFI16*) was also implicated in activation of innate immune response, cellular response to interferons, apoptosis, cell differentiation, and other functions, but unlike *Vnn1* it is strongly down-regulated in *E3hom* mice (LFC = −33.0). Importantly, IFI16/IFI204 is considered to be a part of the inflammasome system (42). The NCBI database lists many functions for Ifi204/IFI16, yet their exact roles in MG are not clear.

While discussing abnormal *E3hom* meibum, it is important to mention recent observations on the microbiome of the ocular surface and MG which emphasize the need to control its diversity (43) and earlier reports that suggested that 1) certain bacteria are susceptible to the anti-microbial properties of meibum (10), and 2) changes in meibum composition can lead to variations in bacterial colonization (44). The abnormal *E3hom* meibum could have diminished antimicrobial properties which might lead to ulceration of the eyelid that is seen even in young 3-months old mice. It remains to be determined if adverse changes in the lipid composition of *E3hom* meibum do contribute to abnormal bacterial flora and/or bacterial load resulting in the ulceration and inflammation of the MGs, conjunctiva and eyelids.

Impact of *Elovl3* inactivation on composition and thermotropic characteristics of meibum.

Central to this discussion is a hypothesis that the chemical composition of meibum, and, hence, activity of the enzymes that are involved in meibogenesis, must be tightly controlled by various physiological regulatory mechanisms, possibly via negative or positive feedback regulation, to maintain the MG lipid homeostasis and physicochemical properties of meibum within acceptable limits. Therefore, changes in meibogenesis induced by *Elovl3* inactivation were evaluated from this standpoint. Also of importance is the acknowledgement of the fact that many of the enzymes listed below are insufficiently characterized and may be multifunctional being involved in two or more types of reactions with other types of substrates (e.g., KAR/HSD17B2). Thus, our discussion is based only on established information and currently prevailing views with regard to the substrate/product specificity of those enzymes.

Inactivation of *Elovl3* caused a dramatic shift in the chemical composition of meibum of *E3hom* mice compared with their heterozygous and wild-type littermates (16). As ELOVL3 is the main enzyme in the FA elongation cycle that acts on C_{16}-C_{20} FA (which are of either dietary origin, or products of ELOVL6) to form homologs longer than C_{20}, its inactivation interrupted the normal course of meibogenesis and led to a decline in C_{20} to C_{28} FA and FAl-based WE, CE, and OAHFA, and accumulation of their shorter chain variants. This effect is most pronounced for saturated and mono-unsaturated FA and FAl, but is minimal or reversed for di- and polyunsaturated ones. Indeed, inactivation of *Elovl3* led to preferential accumulation of di- and polyunsaturated WE with more than 45 carbons at the expense of saturated and mono-unsaturated compounds (16) showing that there might be a bypass from ELOVL6 and/or ELOVL5 and ELOVL7 directly to ELOVL1 that allows to compensate, to a degree, the lack of ELOVL3 (Figure 9).

An important observation was made for meibomian CE: Saturated CE with FA moieties longer than C_{20} were not detected in meibum of *E3hom* mice, while the profile of very and extremely long chain mono-unsaturated CE remained virtually unchanged (16). At the same time, saturated, but branched, CE shorter than $C_{20:0}$ were prominent constituents of the CE pool [Figures 7 and 8 and (28)]. Furthermore, branching of FA considerably lowers melting points of isobaric CE – e.g., cholesteryl ester of methyl branched isostearic acid [or cholesteryl (9-methyl)-heptadecanoate] has a melting point of 25–30°C, while its linear isobaric isomer melts at >80°C (45). Also, the shorter or more unsaturated the lipid in a series of homolog compounds, the lower its melting temperature (31, 46). These three factors – shortening the average lipid chain length of saturated and monounsaturated lipids, the increase in di- and polyunsaturated compounds, and the increase in the molar fraction of branched lipids, – apparently led to the decrease in the meibum melting temperature that was observed in our experiments (Figure 5). The drop in the main transition temperature $\boldsymbol{T_2}$ (Table 1) approached 10 °C which almost completely liquefied meibum of *E3hom* mice at the corneal physiological temperature of ~37 °C. Note that meibum of wild-type mice is in a liquid-crystal, birefringent state at that temperature, and so is human meibum at 32°C (5), which is a normal physiological corneal temperature of humans (47, 48).

Another important observation was a change in the cooperativity of melting. In our earlier experiments we demonstrated that human and mouse meibum behaved in a cooperative manner in several conditions, including melting in expressed state (5, 49, 50), melting inside the MG ducts (5) and in Langmuir trough experiments as a thin film deposited onto the aqueous subphase (50). Later, the cooperative behavior of Meibomian lipids was observed in an independent study (51). In our current experiments, wild-type meibum underwent transition from crystal to liquid-crystal and then to liquid state in a considerably narrower range of temperatures than the *E3hom* meibum, which resulted in a shift in the Hill coefficients ***k*** and ***m*** caused by the mutation toward lower numbers. Cooperativity of lipid melting routinely depends on the degree of crystallization of the sample. The latter, in turn, depends on the ability of its molecules to form regularly organized and tightly packed aggregates held together mainly by Van der Waals forces (or dipole-dipole interactions) and, for ionizable lipids, electrostatic interactions between anions and cations. Saturated straight chain lipids form crystals more easily than their unsaturated and branched analogs which tend to be more disorganized and packed less densely. Thus, the increase in the degree of unsaturation of *Elovl3*-null meibum (16) can be one of the factors that broadened its melting range. These factors cause meibum of *E3hom* mice to melt at much lower temperature than *E3wt* meibum and contribute to its extraordinary fluidity in physiological conditions.

Note that model (Eq. 1) used to analyze thermotropic properties of meibum does not discriminate between two different scenarios: The existence of 1) two partially melted pools of meibum with the same compositions, but different aggregation states, and 2) two pools of meibomian lipids with different compositions and melting characteristics. Both of these explanations are possible, but could not be answered in current experiments and should be evaluated in future experiments.

Impact of *Elovl3* inactivation on MG transcriptome.

Equally significant were alterations in the GEP of meibogenesis-related genes in TPs of *E3hom* mice. As ELOVL3 acts in the middle of the FA elongation cycle (Figure 9), it was reasonable to expect that inactivation of *Elovl3* would influence not only the immediate lipid profiles of ELOVL3, but also the expression patterns of related genes of meibogenesis. Indeed, the changes in the lipid elongation and desaturation patterns were accompanied by noticeable changes in GEP of related genes in *E3hom* TPs (Table 4): Up-regulated with statistical significance were essential genes of the FA biosynthesis and elongation such as *Acat1*, *Acsbg1*, *Acat3*, *Tecr*, *Hacl1*, *Hacd2*, *Hacd3*, and *Elovl1*, while *Hsd17b10*, *Hacd4*, *Hacd1*, and *Elovl7* were down-regulated. Interestingly, other members of the *Elovl* family – *Elovl2*, *Elovl4*, *Elovl5*, and *Elovl6,* – were affected to a much lesser degree, or remained unchanged.

An increase in *Elovl1* and a decrease in *Elovl7* could be interpreted as a response to, or a mechanism to compensate for, the lack of ELOVL3 activity. Indeed, ELOVL1 has a substrate/product specificity that partially overlaps with that of ELOVL3 (16, 52), and could be up-regulated if insufficient production of ELOVL3 products is detected. At the same time, ELOVL7 is involved in biosynthesis of unsaturated VLC FA (53), which are present in excess in *E3hom* meibum (Figure 8 and (16)]. This change in the *Elovl7* expression level

could be an indication of the existence of a negative feedback regulatory/signaling mechanism that regulates the level of unsaturated FA and FAl in TP of mice. Indicatively, the level of expression of another major *Elovl* in the TP – *Elovl6* (19) – was barely influenced by the *Elovl3* mutation. As ELOVL6 catalyzes elongation of short chain FA to form their C_{16} and C_{18} homologs, which were abundantly present in the TEKLAD 2016 mouse diet as essential nutrients, there might have been no need for the regulation of its levels in the TP of *E3hom* mice.

This hypothesis is supported by our earlier observations on the unaffected levels of unsaturated ELOVL4 products (such as ELC CE, OAHFA and Chl-OAHFA) in meibum of *E3hom* mice (16), which are downstream of ELOVL6, ELOVL3 and ELOVL1 enzymes. It seems that the biosynthesis of ultra-long chain FA that is catalyzed by ELOVL4 does not rely exclusively on ELOVL3 products and utilizes those of ELOVL6 and ELOVL1 that can be obtained via a bypass pathway instead (Figure 9).

A related process in meibogenesis is FA desaturation. Inactivation of *Elovl3* caused a minimal, but statistically significant increase in *Fads6*, which encodes a fatty acid desaturase type 6, and *Scd2* – a gene encoding stearoyl CoA desaturase type 2, – but not in other desaturases, which were largely unaffected (Table 5). Note that all four *Scd* genes that are present in mice, *Scd1* through *Scd4*, are normally detected at equally high levels: In *E3wt* mice, microarray expression levels on a log2 scale for all four variants were 18.5–19.9 (20). Their LFC in response to the mutation were all within ±1.4, which is rather minimal. It seems that there was no an effective feedback regulatory mechanism that would control the excessive accumulation of unsaturated lipids in meibum of *E3hom* mice, or the magnitude of the changes induced by the mutation was overwhelmingly high.

One of the affected groups of genes were those related to FA branching, such as *Bckdha*, *Dbt*, and, especially, *Bckdhb* which was upregulated with a LFC of 21 (Table 6). These enzymes play a key role in metabolism of branched chain amino acids, such as leucine, isoleucine, and valine. Importantly, these amino acids (in the form of their *iso*-valeryl-CoA, 2-methyl-butyryl-CoA, and *iso*-butyryl-CoA metabolites) are precursors of *iso*- and *anteiso*-branched FA, which are abundantly present in human and mouse meibomian lipids (1, 19, 28, 30). *Bckdhb* gene encodes a branched-chain alpha-keto acid decarboxylase E1 component of a branched chain alpha-keto dehydrogenase multienzyme complex. The complex catalyzes transformation of alpha-keto acids to branched acyl-CoA and CO_2 which was reported, among other functions, to be required for the biosynthesis of methyl-branched FA (54). Another gene/enzyme pair from that group – *Pcca*/PCCA, or propionyl CoA carboxylase, alpha polypeptide, - was shown to stimulate the synthesis of odd-chain FA (55) which are largely branched in human (30) and bovine (1) meibum. Earlier BCKDHA/BCKDHB family of enzymes was proposed to be an integral part of meibogenesis (19). Their downstream products – branched FA of the C_{14}-C_{20} variety – are mostly saturated and are incorporated into WE (30) and CE (19, 28). Both *Bckdha* and *Bckdhb* are upregulated in *E3hom* mice (Table 6), but the most considerable increase was observed for *Bckdhb* (LFC = 21.1). Indicatively, one of their putative products – branched $C_{17:0}$-FA – was found as a major component of *E3hom* CE (not shown). Applying the same reasoning as for *Elovl7*/*Elovl1*, one may speculate that upregulation of genes related to FA branching was a

physiological response for the absence of ELOVL3 in an attempt to compensate for the lack of ELOVL3 products (mostly, saturated FA) that were to be incorporated in WE and CE. Controversially, *Acox2* (a branched chain acyl-CoA oxidase 2) was also somewhat upregulated (LFC = 2.8). The peroxisomal enzyme it encodes is involved in degradation of branched long chain FA (56) and bile acids (57). Its deficiency results in accumulation of branched lipids and bile acids in tissues associated with Zellweger syndrome and Refsum's disease (58). The effects of *Elovl3* inactivation on lipid branching and bile acid metabolism have not been fully characterized yet, but the experiments are underway and will be reported separately.

For the biosynthesis of WE and DiAD, essential are enzymes that catalyze reduction of fatty acids into fatty alcohols – FAR1 and FAR2 (29). The statistically significant increase in *Far1* expression level in TP of *E3hom* mice could be interpreted as a response to lower levels of ELOVL3 products in an attempt to maximize production WE and related compounds from available precursors. However, the substrate/product specificity of FAR1 and FAR2 with regard to ELC and ULC FA is yet to be established.

The most upregulated gene of all in TP of *E3hom* mice were *Idi2* (LFC = 271) and its associated pseudogene *Gm9745* (LFC = 231). The *Idi2* gene encodes a peroxisomal enzyme isopentyl-diphosphate delta isomerase 2 that is central to the biosynthesis of Chl and other isoprenoids (59). Indicatively, the transcription levels of a number of other Chl biosynthesis-related genes were also increased (Table 3). This is in line with an increased presence of Chl and CE in *E3hom* meibum compared with the norm, though other factors may have contributed to this effect as well.

Our *in vivo* observations of inflammatory processes in the TP of *E3hom* mice were accompanied with an increase in TP levels of several pro-inflammatory genes, such as *Ifi30*, *Cd68*, *Acp5*, and *zc3h12a* (Table 7). In line with this observation, a *Gpnmb* gene, which acts as a negative regulator of macrophage inflammatory responses (60), was highly down-regulated (LFC = −8.2). A lysosomal protease cathepsin S – a modulator of inflammatory responses in several tissues, – was also significantly suppressed (LFC = −6.9). Recently, inhibition of Cathepsin S with a peptide-based inhibitor was shown to reduce inflammation in lacrimal glands and mitigate ocular manifestations of Sjogren's syndrome, reducing the abundance of CD68-positive lymphocytes (61). The expression of cathepsin S is also induced in response to injury and inflammation in muscles where it participates in remodeling the extracellular matrix, while its deletion minimized the pathological changes in the tissues (62). Thus, down-regulation of its gene *Ctss* could be interpreted as an evidence of a functional link between *Elovl3* and *Ctss* and a physiological response in an attempt to reduce inflammation in the tissues of *E3hom* mice. A similar reasoning can be applied to *Spp1* which also was down-regulated (LFC = −6.7). The functions of other differentially expressed genes that are involved in inflammation are too numerous to be discussed in this paper and are to be addressed in future publications. Generally, these changes in GEP were not as large as those in lipid-metabolism related genes, but were statistically significant, which justifies additional experiments to deconvolute their roles in MG inflammation.

Concluding remarks.

Finally, it is important to recapitulate that inactivation of *Elovl3* caused massive changes not only in the lipid profiles of meibum and its physicochemical properties, but it also disturbed the normal GEP in mouse tarsal plates. The latter revealed functional and/or causative links between *Elovl3*/ELOVL3 and other genes/proteins of meibogenesis and inflammation. Also, it seems that a relatively broad substrate and product specificities of other members of the ELOVL family can partially circumvent, but not fully compensate for, the ablation of *Elovl3*/ELOVL3.

Supplementary Material

Refer to Web version on PubMed Central for supplementary material.

ACKNOWLEDGEMENTS

This work was supported by US National Institutes of Health, National Eye Institute grant R01EY024324 (to I.A.B.) and an unrestricted grant for The Research to Prevent Blindness (NY, NY, USA),

Abbreviations

a.m.u.	atomic mass unit (unitless)
AcN	acetonitrile
APCI	atmospheric pressure chemical ionization
CE	cholesteryl ester(s)
Chl	free cholesterol
Chl-OAHFA	cholesteryl ester(s) of (O)-acylated omega-hydroxy fatty acid(s)
DiAD	diacylated alpha,omega-diol(s)
E3hom	homozygous Elovl3 inactivated mice
E3wt	wild type littermates of E3hom mice
ELC	extremely long chain
FA	fatty acid(s)
FAl	fatty alcohol(s)
FFA	free fatty acid(s)
FWHM	full width at half maximum
GEP	gene expression pattern(s)
H&E	hematoxyline/eosin staine
HSPLM	hot stage cross-polarized light microscopy

IPA	iso-propanol
LFC	linear fold change
m/z	mass-to-charge ratio (unitless)
MG	Meibomian gland(s)
ML	meibomian lipid(s)
NIM	negative ion mode
OAHFA	(O)-acylated omega-hydroxy fatty acid(s)
PCA	Principal Component Analysis
PIM	positive ion mode
RP	reversed phase
TAG	triacyl glycerol(s)
TF	tear film
TFLL	tear film lipid layer
TP	tarsal plate(s)
ULC	ultra long chain
UPLC	ultra high performance chromatography
VLC	very long chain
WE	wax ester(s)

REFERENCES

1. Nicolaides N, Kaitaranta JK, Rawdah TN, Macy JI, Boswell FM 3rd, and Smith RE (1981) Meibomian gland studies: comparison of steer and human lipids. Invest Ophthalmol Vis Sci 20, 522–536 [PubMed: 7194326]
2. McMahon A, Lu H, and Butovich IA (2013) The spectrophotometric sulfo-phospho-vanillin assessment of total lipids in human meibomian gland secretions. Lipids 48, 513–525 [PubMed: 23345137]
3. McCulley JP, and Shine W (1997) A compositional based model for the tear film lipid layer. Trans Am Ophthalmol Soc 95, 79–88; discussion 88–93 [PubMed: 9440164]
4. Brauninger GE, Shah DO, and Kaufman HE (1972) Direct physical demonstration of oily layer on tear film surface. Am J Ophthalmol 73, 132–134 [PubMed: 5007343]
5. Butovich IA, Lu H, McMahon A, Ketelson H, Senchyna M, Meadows D, Campbell E, Molai M, and Linsenbardt E (2014) Biophysical and morphological evaluation of human normal and dry eye meibum using hot stage polarized light microscopy. Invest Ophthalmol Vis Sci 55, 87–101 [PubMed: 24282231]
6. Tsai PS, Evans JE, Green KM, Sullivan RM, Schaumberg DA, Richards SM, Dana MR, and Sullivan DA (2006) Proteomic analysis of human meibomian gland secretions. Br J Ophthalmol 90, 372–377 [PubMed: 16488965]

7. Jeyalatha MV, Qu Y, Liu Z, Ou S, He X, Bu J, Li S, Reinach PS, and Li W (2017) Function of meibomian gland: Contribution of proteins. Exp Eye Res 163, 29–36 [PubMed: 28950937]
8. Mondino BJ, Bath PE, Foos RY, Apt L, and Rajacich GM (1984) Absent meibomian glands in the ectrodactyly, ectodermal dysplasia, cleft lip-palate syndrome. Am J Ophthalmol 97, 496–500 [PubMed: 6720821]
9. Tiffany JM (2008) The normal tear film. Dev Ophthalmol 41, 1–20 [PubMed: 18453758]
10. Mudgil P (2014) Antimicrobial role of human meibomian lipids at the ocular surface. Invest Ophthalmol Vis Sci 55, 7272–7277 [PubMed: 25316725]
11. Villarreal-Gonzalez AJ, Jocelyn Rivera-Alvarado I, Rodriguez-Gutierrez LA, and Rodriguez-Garcia A (2020) Analysis of ocular surface damage and visual impact in patients with primary and secondary Sjogren syndrome. Rheumatol Int
12. Koh S (2016) Mechanisms of Visual Disturbance in Dry Eye. Cornea 35 Suppl 1, S83–S88 [PubMed: 27583799]
13. McCulley JP (1984) Blepharoconjunctivitis. Int Ophthalmol Clin 24, 65–77 [PubMed: 6233233]
14. Suzuki T (2012) Meibomitis-related keratoconjunctivitis: implications and clinical significance of meibomian gland inflammation. Cornea 31 Suppl 1, S41–44 [PubMed: 23038034]
15. Sassa T, Tadaki M, Kiyonari H, and Kihara A (2018) Very long-chain tear film lipids produced by fatty acid elongase ELOVL1 prevent dry eye disease in mice. Faseb J 32, 2966–2978 [PubMed: 29401594]
16. Butovich IA, Wilkerson A, Bhat N, McMahon A, and Yuksel S (2019) On the pivotal role of Elovl3/ELOVL3 in meibogenesis and ocular physiology of mice. Faseb J 33, 10034–10048 [PubMed: 31208226]
17. Miyamoto M, Sassa T, Sawai M, and Kihara A (2020) Lipid polarity gradient formed by omega-hydroxy lipids in tear film prevents dry eye disease. Elife 9
18. Miyazaki M, Man WC, and Ntambi JM (2001) Targeted disruption of stearoyl-CoA desaturase1 gene in mice causes atrophy of sebaceous and meibomian glands and depletion of wax esters in the eyelid. J Nutr 131, 2260–2268 [PubMed: 11533264]
19. Butovich IA, McMahon A, Wojtowicz JC, Lin F, Mancini R, and Itani K (2016) Dissecting lipid metabolism in meibomian glands of humans and mice: An integrative study reveals a network of metabolic reactions not duplicated in other tissues. Biochim Biophys Acta 1861, 538–553 [PubMed: 27032494]
20. Butovich IA, McMahon A, Wojtowicz JC, Bhat N, and Wilkerson A (2019) Effects of sex (or lack thereof) on meibogenesis in mice (Mus musculus): Comparative evaluation of lipidomes and transcriptomes of male and female tarsal plates. Ocul Surf 17, 793–808 [PubMed: 30890458]
21. Butovich IA (2009) Lipidomic analysis of human meibum using HPLC-MSn. Methods Mol Biol 579, 221–246 [PubMed: 19763478]
22. Vogel B, Wagner H, Gmoser J, Worner A, Loschberger A, Peters L, Frey A, Hofmann U, and Frantz S (2016) Touch-free measurement of body temperature using close-up thermography of the ocular surface. MethodsX 3, 407–416 [PubMed: 27284532]
23. Butovich IA, Bhat N, and Wojtowicz JC (2019) Comparative Transcriptomic and Lipidomic Analyses of Human Male and Female Meibomian Glands Reveal Common Signature Genes of Meibogenesis. Int J Mol Sci 20, 4539
24. Butovich IA (2017) Meibomian glands, meibum, and meibogenesis. Exp Eye Res 163, 2–16 [PubMed: 28669846]
25. Butovich IA, Uchiyama E, and McCulley JP (2007) Lipids of human meibum: mass-spectrometric analysis and structural elucidation. J Lipid Res 48, 2220–2235 [PubMed: 17626978]
26. Jump DB (2009) Mammalian fatty acid elongases. Methods Mol Biol 579, 375–389 [PubMed: 19763486]
27. Kihara A (2012) Very long-chain fatty acids: elongation, physiology and related disorders. J Biochem 152, 387–395 [PubMed: 22984005]
28. Yuksel S, Bhat N, Wilkerson A, McMahon A, Wojtowicz J, and Butovich IA (2019) Side-by-side comparison of branching and elongation patterns of cholesteryl esters of human and mouse meibum In ARVO-2019 Vol. 60 p. 4175, Invest Ophthalmol Vis Sci, Vancouver, Canada

29. Cheng JB, and Russell DW (2004) Mammalian wax biosynthesis. I. Identification of two fatty acyl-Coenzyme A reductases with different substrate specificities and tissue distributions. J Biol Chem 279, 37789–37797 [PubMed: 15220348]
30. Butovich IA, Arciniega JC, Lu H, and Molai M (2012) Evaluation and quantitation of intact wax esters of human meibum by gas-liquid chromatography-ion trap mass spectrometry. Invest Ophthalmol Vis Sci 53, 3766–3781 [PubMed: 22531701]
31. Knothe G, and Dunn RO (2009) A Comprehensive Evaluation of the Melting Points of Fatty Acids and Esters Determined by Differential Scanning Calorimetry. Journal of the American Oil Chemists Society 86, 843–856
32. Cason J (1948) Branched-chain fatty acids; relationship of melting point to structure; new method of synthesis of acids containing a quaternary carbon atom. J Org Chem 13, 227–238 [PubMed: 18903739]
33. Iyengar BT, and Schlenk H (1969) Melting points of synthetic wax esters. Lipids 4, 28–30 [PubMed: 5766845]
34. Andres-Benito P, Moreno J, Dominguez R, Aso E, Povedano M, and Ferrer I (2017) Inflammatory Gene Expression in Whole Peripheral Blood at Early Stages of Sporadic Amyotrophic Lateral Sclerosis. Front Neurol 8, 546 [PubMed: 29081763]
35. Lamort AS, Giopanou I, Psallidas I, and Stathopoulos GT (2019) Osteopontin as a Link between Inflammation and Cancer: The Thorax in the Spotlight. Cells 8
36. Reneker LW, Irlmeier RT, Shui YB, Liu Y, and Huang AJW (2020) Histopathology and selective biomarker expression in human meibomian glands. Br J Ophthalmol 104, 999–1004 [PubMed: 31585964]
37. Berdyshev E, Goleva E, Bronova I, Dyjack N, Rios C, Jung J, Taylor P, Jeong M, Hall CF, Richers BN, Norquest KA, Zheng T, Seibold MA, and Leung DY (2018) Lipid abnormalities in atopic skin are driven by type 2 cytokines. JCI Insight 3
38. McMahon A, Butovich IA, and Kedzierski W (2011) Epidermal expression of an Elovl4 transgene rescues neonatal lethality of homozygous Stargardt disease-3 mice. J Lipid Res 52, 1128–1138 [PubMed: 21429867]
39. Keyes BE, Liu S, Asare A, Naik S, Levorse J, Polak L, Lu CP, Nikolova M, Pasolli HA, and Fuchs E (2016) Impaired Epidermal to Dendritic T Cell Signaling Slows Wound Repair in Aged Skin. Cell 167, 1323–1338 e1314 [PubMed: 27863246]
40. Jansen PA, Kamsteeg M, Rodijk-Olthuis D, van Vlijmen-Willems IM, de Jongh GJ, Bergers M, Tjabringa GS, Zeeuwen PL, and Schalkwijk J (2009) Expression of the vanin gene family in normal and inflamed human skin: induction by proinflammatory cytokines. J Invest Dermatol 129, 2167–2174 [PubMed: 19322213]
41. Berruyer C, Pouyet L, Millet V, Martin FM, LeGoffic A, Canonici A, Garcia S, Bagnis C, Naquet P, and Galland F (2006) Vanin-1 licenses inflammatory mediator production by gut epithelial cells and controls colitis by antagonizing peroxisome proliferator-activated receptor gamma activity. J Exp Med 203, 2817–2827 [PubMed: 17145956]
42. Wang B, and Yin Q (2017) AIM2 inflammasome activation and regulation: A structural perspective. J Struct Biol 200, 279–282 [PubMed: 28813641]
43. Suzuki T, Sutani T, Nakai H, Shirahige K, and Kinoshita S (2020) The Microbiome of the Meibum and Ocular Surface in Healthy Subjects. Invest Ophthalmol Vis Sci 61, 18
44. McCulley JP, and Shine WE (2003) Meibomian gland function and the tear lipid layer. Ocul Surf 1, 97–106 [PubMed: 17075642]
45. Urata K, and Takaishi N (1997) Cholesteryl ester compounds containing alkyl branched acyl groups — their preparations, properties and applications. Lipid / Fett 99, 327–332
46. Ginsburg GS, Atkinson D, and Small DM (1984) Physical Properties of Cholesteryl Esters. Prog Lipid Res 23, 135–167 [PubMed: 6399750]
47. Morgan PB, Tullo AB, and Efron N (1995) Infrared thermography of the tear film in dry eye. Eye (Lond) 9 (Pt 5), 615–618 [PubMed: 8543082]
48. Efron N, Young G, and Brennan NA (1989) Ocular surface temperature. Curr Eye Res 8, 901–906 [PubMed: 2791634]

49. Lu H, Wojtowicz JC, and Butovich IA (2013) Differential scanning calorimetric evaluation of human meibomian gland secretions and model lipid mixtures: transition temperatures and cooperativity of melting. Chem Phys Lipids 170–171, 55–64
50. Butovich IA, Arciniega JC, and Wojtowicz JC (2010) Meibomian lipid films and the impact of temperature. Invest Ophthalmol Vis Sci 51, 5508–5518 [PubMed: 20610839]
51. Sledge S, Henry C, Borchman D, Yappert MC, Bhola R, Ramasubramanian A, Blackburn R, Austin J, Massey K, Sayied S, Williams A, Georgiev G, and Schikler KN (2017) Human Meibum Age, Lipid-Lipid Interactions and Lipid Saturation in Meibum from Infants. Int J Mol Sci 18
52. Mueller N, Sassa T, Morales-Gonzalez S, Schneider J, Salchow DJ, Seelow D, Knierim E, Stenzel W, Kihara A, and Schuelke M (2019) De novo mutation in ELOVL1 causes ichthyosis, acanthosis nigricans, hypomyelination, spastic paraplegia, high frequency deafness and optic atrophy. J Med Genet 56, 164–175 [PubMed: 30487246]
53. Shi H, Wang L, Luo J, Liu J, Loor JJ, and Liu H (2019) Fatty Acid Elongase 7 (ELOVL7) Plays a Role in the Synthesis of Long-Chain Unsaturated Fatty Acids in Goat Mammary Epithelial Cells. Animals (Basel) 9
54. Jia F, Cui M, Than MT, and Han M (2016) Developmental Defects of Caenorhabditis elegans Lacking Branched-chain α-Ketoacid Dehydrogenase Are Mainly Caused by Monomethyl Branched-chain Fatty Acid Deficiency. Journal of Biological Chemistry 291, 2967–2973
55. Sperl W, Murr C, Skladal D, Sass JO, Suormala T, Baumgartner R, and Wendel U (2000) Odd-numbered long-chain fatty acids in propionic acidaemia. Eur J Pediatr 159, 54–58 [PubMed: 10653330]
56. Ferdinandusse S, Denis S, van Roermund CWT, Preece MA, Koster J, Ebberink MS, Waterham HR, and Wanders RJA (2018) A novel case of ACOX2 deficiency leads to recognition of a third human peroxisomal acyl-CoA oxidase. Biochim Biophys Acta Mol Basis Dis 1864, 952–958 [PubMed: 29287774]
57. Vilarinho S, Sari S, Mazzacuva F, Bilguvar K, Esendagli-Yilmaz G, Jain D, Akyol G, Dalgic B, Gunel M, Clayton PT, and Lifton RP (2016) ACOX2 deficiency: A disorder of bile acid synthesis with transaminase elevation, liver fibrosis, ataxia, and cognitive impairment. Proc Natl Acad Sci U S A 113, 11289–11293 [PubMed: 27647924]
58. Singh H, Usher S, Johnson D, and Poulos A (1990) A comparative study of straight chain and branched chain fatty acid oxidation in skin fibroblasts from patients with peroxisomal disorders. J Lipid Res 31, 217–225 [PubMed: 1691260]
59. Nakamura K, Mori F, Tanji K, Miki Y, Yamada M, Kakita A, Takahashi H, Utsumi J, Sasaki H, and Wakabayashi K (2015) Isopentenyl diphosphate isomerase, a cholesterol synthesizing enzyme, is localized in Lewy bodies. Neuropathology 35, 432–440 [PubMed: 25950736]
60. Ripoll VM, Irvine KM, Ravasi T, Sweet MJ, and Hume DA (2007) Gpnmb is induced in macrophages by IFN-gamma and lipopolysaccharide and acts as a feedback regulator of proinflammatory responses. J Immunol 178, 6557–6566 [PubMed: 17475886]
61. Klinngam W, Janga SR, Lee C, Ju Y, Yarber F, Shah M, Guo H, Wang D, MacKay JA, Edman MC, and Hamm-Alvarez SF (2019) Inhibition of Cathepsin S Reduces Lacrimal Gland Inflammation and Increases Tear Flow in a Mouse Model of Sjogren's Syndrome. Sci Rep 9, 9559 [PubMed: 31267034]
62. Tjondrokoesoemo A, Schips TG, Sargent MA, Vanhoutte D, Kanisicak O, Prasad V, Lin SC, Maillet M, and Molkentin JD (2016) Cathepsin S Contributes to the Pathogenesis of Muscular Dystrophy in Mice. J Biol Chem 291, 9920–9928 [PubMed: 26966179]
63. Wilkerson A, Bhat N, McMahon A, and Butovich IA (2019) Elongase of very long chain fatty acids-3 (ELOVL3) is critical for meibum biosynthesis in mice In ARVO-2019 Vol. 60 p. 4194, Invest Ophthalmol Vis Sci, Vancouver, Canada

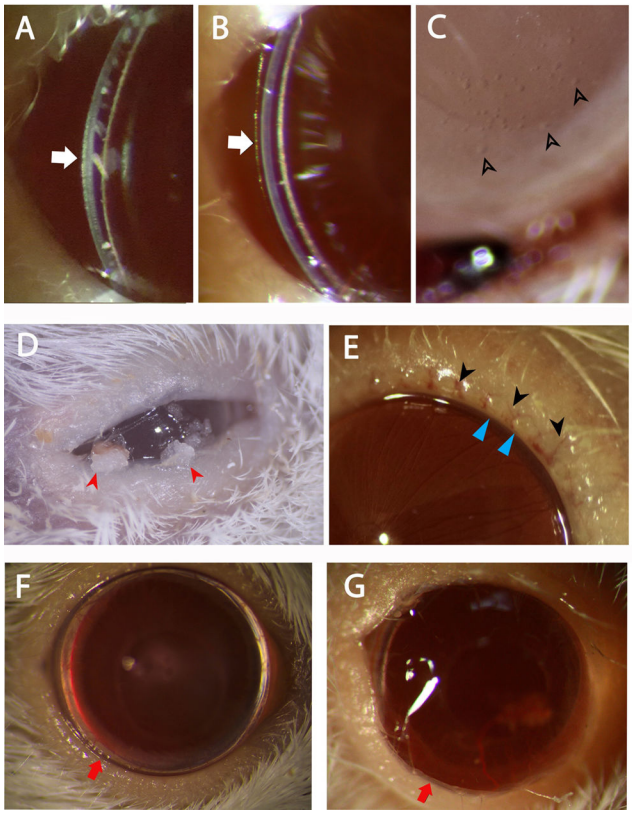

Figure 1. Ocular phenotypes of E3wt and E3hom mice.

Panel A: Tear film (white arrow) and corneal epithelium of a 13-month old *E3wt* mouse. *Panel B: E3hom* corneal section illustrating thickened tear film (white arrow) in a 13-month old mutant mouse; *PanelC:* Clear oil-like droplets (black arrowheads) within the tear film and irritated conjunctiva (red tissues, out of focus) of a 3-month old *E3hom* mouse; *Panel D:* Crusty lipid-like deposits (red arrowheads) and swollen eyelids of a 18-month old *E3hom* mouse; *Panel E:* Enlarged Meibomian gland orifices (blue triangles) and dilated blood vessels of the eyelid margin (black arrowheads) of a 3 month-old *E3hom* mouse; *Panel F:* Normal eye of a 18 month-old *E3wt* mouse with a thin eyelid margin lack excessive conjunctiva (red arrow), hair loss, and corneal neovascularization; *Panel G:* Pooling of the tear film with a conjunctival fold on the lower eyelid margin, corneal vascularization (red arrow) and partial hair loss in a 18 month-old *E3hom* mouse.

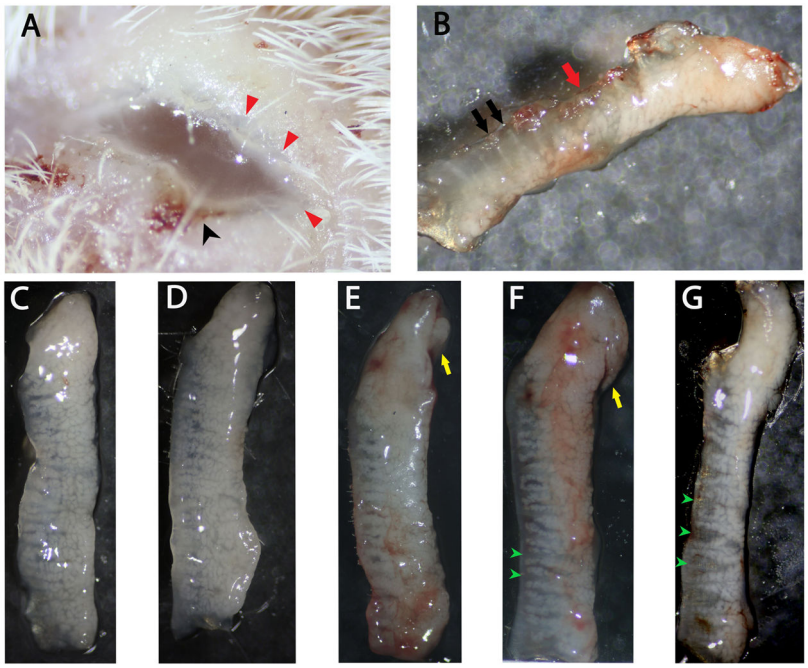

Figure 2. Tarsal plate characteristics of E3hom and E3wt mice.

Panel A: Milky tear film of a 3-month old mouse with excessive accumulation of liquid around the eyelid margins (red triangle) and eyelid ulceration (black arrowhead). *Panel B*: Tarsal plate of a mouse shown in Panel A with distinct central ducts (black arrows) and no Meibomian gland dropout. *Panels C and D*: *E3wt* upper (C) and lower (D) tarsal plates with even distribution of acini throughout the tarsal plate. *Panels E and F*: *E3hom* upper (E) and lower (F) tarsal plates with regularly spaced orifices (green arrows) and abnormally long ascini (yellow arrow). *Panel G*: Lower tarsal plate of a *E3hom* mouse with irregularly spaces (gapping) Meibpmian gland orifices (green arrowheads).

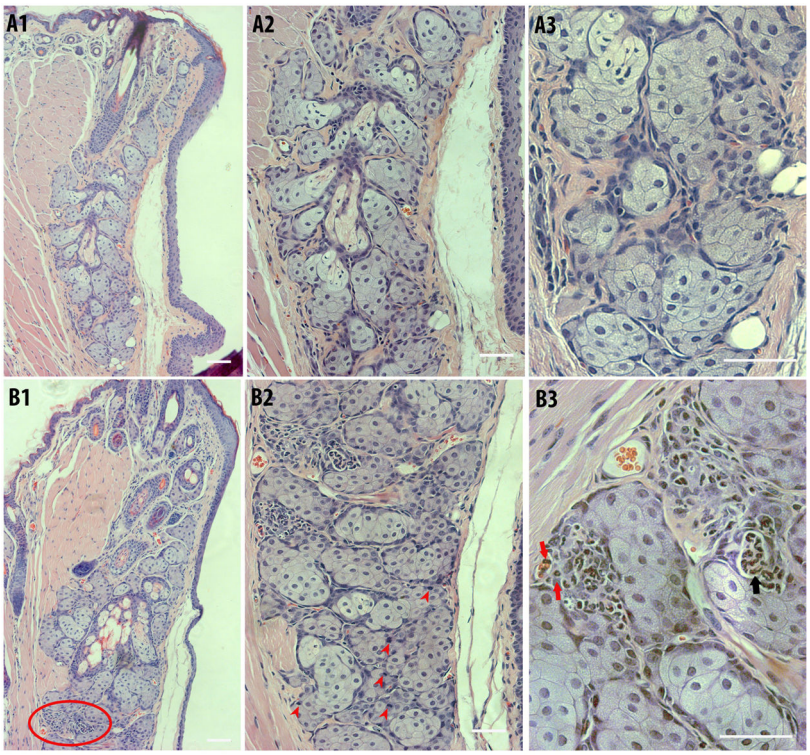

Figure 3. Histological evaluation of tarsal plates of 3 month old E3wt and E3hom mice.

Panels A1-A3: Histological features of *E3wt* tarsal plates. *Panels B1-B3*: Tarsal plates of a *E3hom* mouse displaying accumulation of pro-inflammatory cells (red circle; *B1*) with numerous mitotic figures within the acini (red arrowheads; *B3*). Pro-inflammatory cells within the blood vessel and acinar tissue (red arrows; *B3*) and amassed neutrophils (black arrow; *B3*). H&E staining. Scale bars: 100μm (Panels *A1-A2*; *B1-B2*) and 50μm (Panels *A3* and *B3*).

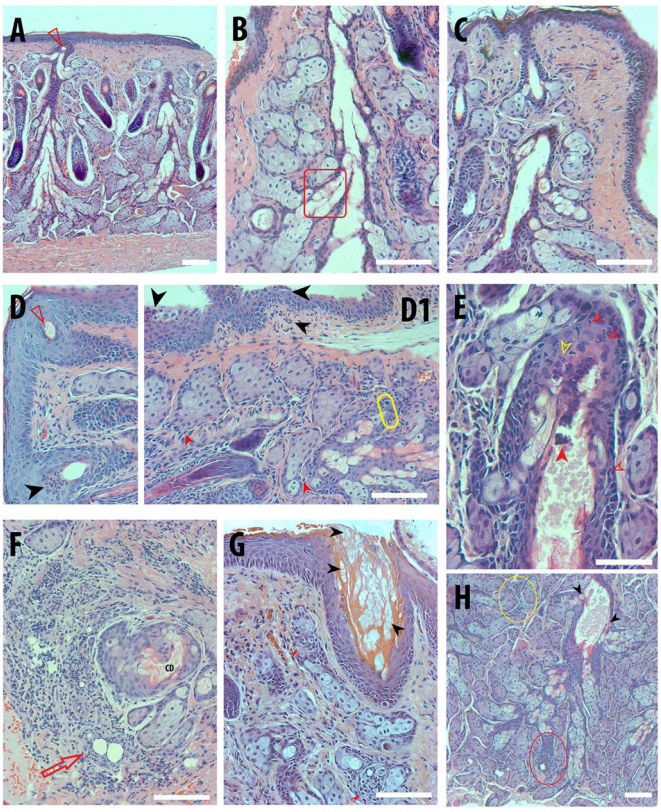

Figure 4. Histological comparison of ocular tissues of aging E3wt and E3hom mice.

Panel A: *E3wt* mice demonstrated normal MG features without noticeable age related changes and no obstruction of the orifice (red triangle). *Panels B, C*: *E3wt* with no retention of cellular membrane in the disintegration zone (red square) with distinct epithelial cells of the thin ductal epithelium. *Panel D*: *E3hom* tarsal plate with inflammation of the hair follicle (black arrowhead) and retention of debris within the orifice (red triangle) at 8 months old. *Panel D1*: Inflammation of the conjunctiva (black arrowheads) and surrounding the MG (red arrowheads) and mitotic cells (yellow circle). *Panel E*: *E3hom* thickened central duct with inflammatory cells within the ductal epithelium (yellow arrowhead), nuclear remnants (open red arrowhead) and amorphous cellular debris (solid red arrowhead). *Panel F*: Substantial inflammation surrounding the MG with large clear spaces (red arrow) that resembles a lipogranulomatous inflammation (e.g. chalazion) in *E3hom* TP. *Panel G: E3hom* orifice with bright eosinophilic material that resembles intact duct material and cellular membranes of meibocytes (black arrowheads) with inflammation of the acini (red arrowheads). *Panel H*: Numerous acini with inflammation of acini (red circle) and periacinal space (yellow circle) with incomplete disintegration at the connecting duct and central duct junction (black arrowheads) in *E3hom* MGs. Scale bars: 100μm (all panels) and 50μm (Panel E).

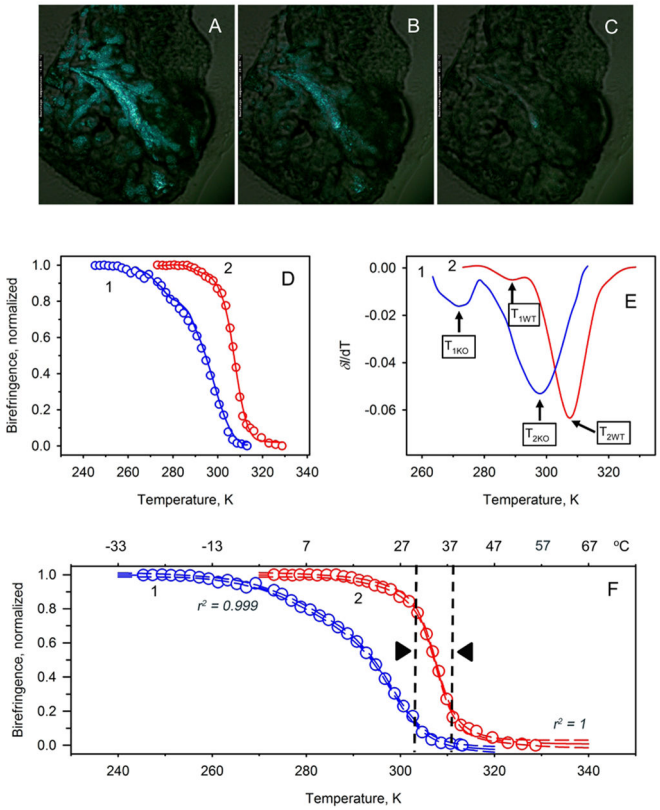

Figure 5. Evaluation of thermotropic characteristics of E3wt and E3hom meibum using hot stage cross-polarized lighr microscopy.

Panels A-C: A tissue section of a tarsal plate of a *E3wt* mouse at, respectively, −4.8°C, 29.9°C, and 40.1°C. Disappearing bright birefringent structures inside acini and ducts is meibum that undergoes gradual transition from (liquid)-crystal to liquid state. *Panel D:* Intensity of birefringence of *E3hom* (blue; 1) and *E3wt* (red; 2) meibum as function of sample temperature. Dots - experimental values; lines – spline approximation of experimental data). Data extracted from the data files as described in (5). *Panel E:* Numerically differentiated melting curves of *E3hom* (blue; 1) and *E3wt* (red; 2) from Panel D. *Panel F:* Experimental data (dots) from Panels D approximated using Equation 1 assuming a three-phase, two-transitions model of meibum melting (solid lines). Mouse corneal physiological temperature limits are marked with black triangles. Note that *E3hom* meibum is almost completely melted at above 30°C, while *E3wt* meibum remains in predominantly liquid-crystal state.

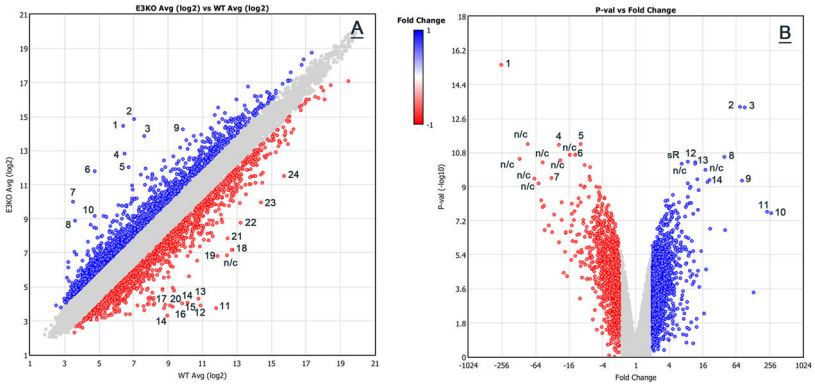

Figure 6. Comparative transcriptomic characterization of tarsal plates of E3wt (n=4) and E3hom (n=6) mice.

Panel A: A *E3hom*-vs.-*E3wt* scatter plot with differentially expressed genes colored in blue (upregulated) and red (down-regulated) in *E3hom* mice. The grey area represents a pool of genes that did not match standard statistical criteria: Fold Change: < (−2) or > (+2); $p \leq 0.05$. The following genes are labeled: 1) *Idi2*; 2) *Gm9745*; 3) *Eno1b*; 4) *Pla2g4e*; 5) *Rpl10a-ps2*; 6) *Bc048546*; 7) *Psg29*; 8) *H2-Ea-ps*; 9) *Bckdhb*; 10) *Plppr2*; 11) *Skint3*; 12–16) non-coding; 17) *Trim12a*; 18) *Gm10462*; 19) *Ifi204*; 20) *Pbp2*; 21) *Pla2g2f*; 22) *Pvalb*; 23) *Actn3*: 24) *Lyz2*.

Panel B: A P-val. Vs. Fold Change Volcano plot for *E3hom* and *E3wt* mice. 1) *Skint*; 2) *Eno1b*; 3) *Psg29*; 4) *Pla2g2f*; 5) *Minos1*; 6) *Hist1h4c*; 7) *Ifi204*; 8) *H2-Ea-ps*; 9) *Pla2g4e*; 10) *Idi2*; 11) *Gm9745*; 12) *Alad*; 13) *Cyp2b10*; 14) *Bckdhb*; 15) *Snord93*; sR – small RNA; n/c – non-coding RNA.

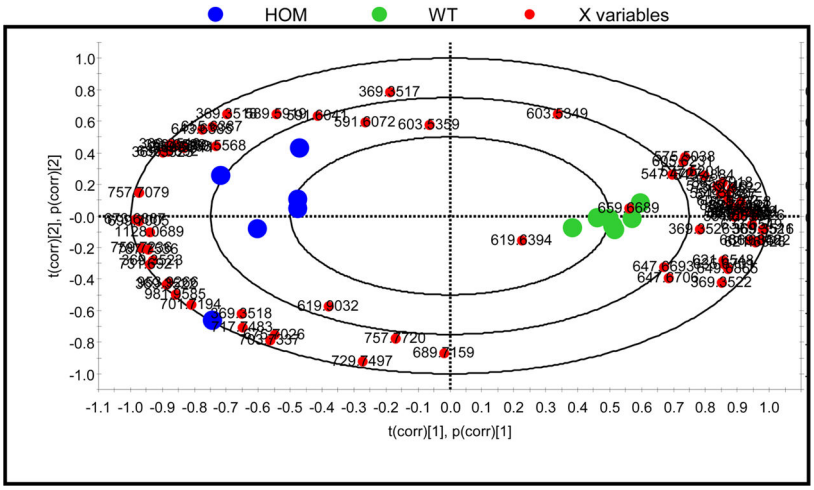

Figure 7. Loadings bi-plot of the results of Unsupervised Principal Component analysis of E3hom (n=6; blue) and E3wt (n=7; green) tarsal plate samples.

Reverse phase UPLC/APCI MS analyses of 6 *E3hom* and 7 wild type mice were conducted. Note tight grouping of the specimens of the same type and clear inter-group separation of *E3hom* and *E3wt* specimens. A close look at the graph revealed that *E3wt* samples co-localized with wax esters and long-chain cholesteryl esters, while *E3hom* samples – with shorter-chain cholesteryl esters and triacylglycerols. Additional information on the lipid profiles of these mice can be found in (16, 63).

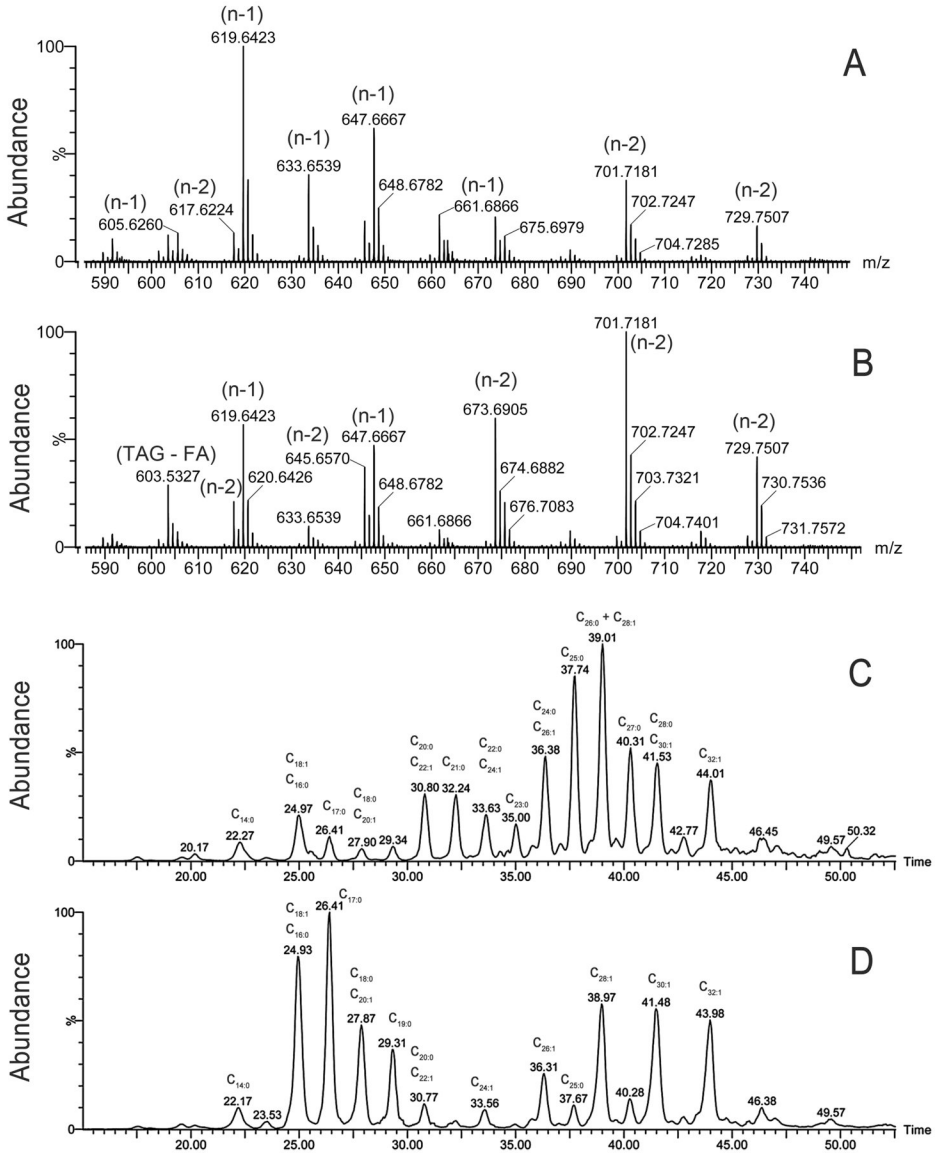

Figure 8. Evaluation of mouse meibum wax esters and cholesteryl esters using liquid chromatography/high resolution mass spectrometry in positive ion mode.

Wax ester fractions of *E3wt* (*Panel A*) and *E3homPanel B* meibum. Partial mass spectra with the signals of mono-unsaturated (n−1) and di-unsaturated (n−2) wax esters are shown. Note a substantial increase in di-unsaturated/mono-unsaturated wax ratio in *E3hom* mice. Meibomian cholesteryl esters of *E3wt* (*Panel C*) and *E3hom* (*Panel D)* mice. The samples from mutant mice had abnormally high levels of shorter chain CE compared with their wild-type littermates, whose cholesteryl esters were based on considerably longer fatty acids.

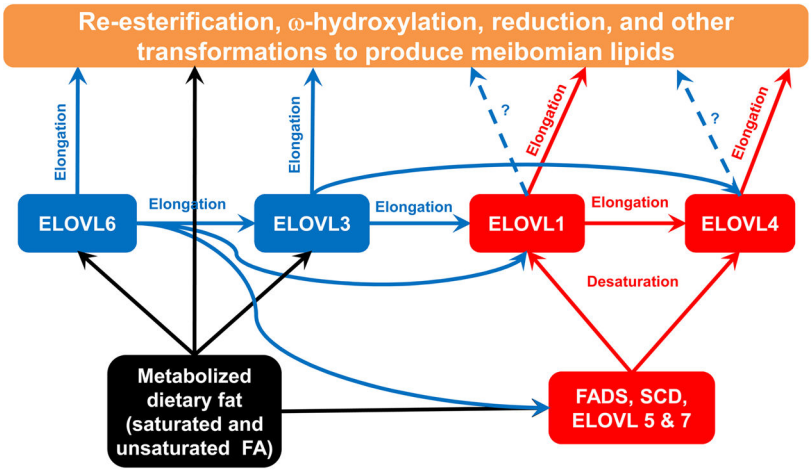

Figure 9. The elongation and desaturation core of saturated (blue) and unsaturated (red) fatty acids in Meibomian glands.

Blue question marks indicate hypothetical links. For more detailed discussion on meibogenesis see our earlier papers (16, 19, 20, 23, 24).

Table 1.

Melting characteristics of representative samples of meibum in tarsal plates of *E3wt* and *E3hom* mice illustrated in Figure 5.

Type of meibum	*A*	*B*	*C*	*k*	*m*	T_1 (K)	T_1 (°C)	T_2 (K)	T_2 (°C)	r^2	F_{stat}
E3wt	1	0.11	0.89	116	129	290.4	17.3	307.7	34.6	0.999	4.2×10^3
E3hom	1	0.16	0.84	85	59	272.6	−0.6	297.1	24.0	1	4.6×10^4

Table 2.

Overall effects of *Elovl3* inactivation on gene expression profiles in tarsal plates of mice.

Transcripts	Detected, total	Passed filter	Up-regulated	Down-regulated
Protein-coding	11,264	779	387	392
Multiple-Complex	15,332	866	485	381
Pseudo-genes	2,758	159	65	94
Non-coding	31,717	1,251	1,043	208

Table 3.

Linear fold changes in the expression levels of core genes of cholesterol biosynthesis and functions in tarsal plates of *E3wt* and *E3hom* mice.

Gene*	Enzyme	EC Number	*E3hom*/*E3wt*, Linear Fold Change**	*p*-value***
Idi2	isopentenyl-diphosphate delta isomerase 2	5.3.3.2	270.9 (↑↑)	**2.48E-08**
Gm9745	*Idi2*-related pseudogene	pseudogene	231.0 (↑↑)	**2.08E-08**
Hmgcs2	3-hydroxy-3-methylglutaryl-CoA synthase 2	2.3.3.10	5.4 (↑)	**8.85E-07**
Vnn1	vanin 1	3.5.1.92	4.29 (↑)	**2.66E-06**
Pmvk	phosphomevalonate kinase	2.7.4.2	4.2 (↑)	**5.23E-06**
Acat3	acetyl-CoA acetyltransferase 3	2.3.1.9	3.6 (↑)	**1.09E-07**
Hmgcr	3-hydroxy-3-methylglutaryl-CoA reductase	1.1.1.34	3.4 (↑)	**3.82E-06**
Mvd	mevalonate (diphospho) decarboxylase	4.1.1.33	2.7 (↑)	**6.50E-05**
Lss	lanosterol synthase	5.4.99.7	2.5 (↑)	**0.0001**
Fdft1	farnesyl diphosphate farnesyl transferase 1 / squalene synthase	2.5.1.21	2.4 (↑)	**0.0015**
Idi1	isopentenyl-diphosphate delta isomerase	5.3.3.2	2.3 (↑)	**0.0017**
Mvk	mevalonate kinase	2.7.1.36	2.1 (↑)	**0.0119**
Msmo1/Sc4mol	methylsterol monoxygenase 1	1.14.18.9	2.1 (↑)	**0.0016**
Lipa	lysosomal acid lipase A / cholesteryl ester hydrolase	3.1.1.13	−2.2 (↓)	**3.39E-05**

*The list assembled from IMPaLA, GeneCards, Brenda and UniProt databases.

**Considerably up- and down-regulated genes are labeled with arrows (↑) and (↓), respectively (if −2≥LFC ≥2 and $p < 0.05$). Highly up-regulated genes (LFC > 10) are labeled with double arrows (↑↑). LFC value of ~1 means no change (NC) regardless of *p*-value.

***p-values of < 0.05 were considered to be statistically significant (in bold).

Table 4.

Changes in expression values of fatty acid elongation-related genes in tarsal plates of *E3wt* and *E3hom* mice.

Gene*	Enzyme*	EC Number*	*E3hom*/*E3wt*, Linear Fold Change**	*p*-value***
Acat2	acetyl-Coenzyme A acetyltransferase 2	2.3.1.9	4.7 (↑)	**3.67E-06**
Acsbg1	acyl-CoA synthetase bubblegum family member 1	6.2.1.3	4.3 (↑)	**6.92E-06**
Acat3	acetyl-CoA acetyltransferase 3	2.3.1.9	3.6 (↑)	**1.09E-07**
Tecr	trans-2,3-enoyl-CoA reductase	1.3.1.93	3.6 (↑)	**0.0002**
Hacl1	2-hydroxyacyl-CoA lyase 1	4.1.2.n2	2.4 (↑)	**0.0001**
Hacd3	3-hydroxyacyl-CoA dehydratase 3	4.2.1.134	2.0 (↑)	**4.01E-06**
Elovl1	ELOVL family member 1	2.3.1.199	1.8 (NC/↑)	**2.89E-05**
Elovl5	ELOVL family member 5	2.3.1.199	1.5 (NC)	0.1186
Elovl6	ELOVL family member 6	2.3.1.199	1.4 (NC)	0.1447
Hacd2	3-hydroxyacyl-CoA dehydratase 2	4.2.1.134	1.3 (NC/↑)	**0.0283**
Kar (Hsd17b12)	very long chain ketoacyl-CoA reductase	1.1.1.330	1.3 (NC)	0.1226
Elovl4	ELOVL family member 4	2.3.1.199	1.0 (NC)	0.9615
Elovl2	ELOVL family member 2	2.3.1.199	−1.1 (NC)	0.2938
Hsd17b10	3-hydroxyacyl-CoA dehydrogenase 2 / hydroxysteroid (17-beta) dehydrogenase 10	1.1.1.178	−1.5 (NC/↓)	**0.0039**
Hacd4	3-hydroxyacyl-CoA dehydratase 4	4.2.1.134	−1.9 (NC/↓)	**0.0048**
Hacd1	3-hydroxyacyl-CoA dehydratase 1	4.2.1.134	−2.0 (↓)	**2.56E-05**
Elovl7	ELOVL family member 3 (does not act on FA >C20)	2.3.1.199	−2.4 (↓)	**1.06E-05**

*The list assembled from IMPaLA, GeneCards, Brenda and UniProt databases.

**Considerably up- and down-regulated genes are labeled with arrows (↑) and (↓), respectively (if −2≥LFC ≥2 and $p < 0.05$). LFC value of ~1 means no change (NC) in the expression values regardless of *p*-value. If 2 ≥LFC ≥ −2 and $p < 0.05$, ambiguous designations (NC/↑) and (NC/↓) were used.

***p-values of < 0.05 were considered to be statistically significant (in bold).

Table 5.

Changes in expression values of core genes of fatty acid desaturation in tarsal plates of *E3wt* and *E3hom* mice.

Gene*	Enzyme*	EC Number*	*E3hom*/*E3wt*, Linear Fold Change**	*p*-value***
Fads6 (diunsat)	fatty acid desaturase domain family, member 6	1.14.19.3	2.4 (↑)	**0.0001**
Scd2(monounsat)	Stearoyl-CoA desaturase 2	1.14.19.1	1.4 (NC/↑)	**0.0005**
Fads2	fatty acid desaturase domain family, member 2	1.14.19.3	1.2 (NC)	0.2456
Scd1	Stearoyl-CoA desaturase 1	1.14.19.1	1.1 (NC)	0.5507
Fads3	fatty acid desaturase domain family, member 3	1.14.19.3	1.0(NC)	0.8495
Scd3	Stearoyl-CoA desaturase 3	1.14.19.1	−1.1 (NC)	0.2555
Fads1	fatty acid desaturase domain family, member 1	1.14.19.3	−1.2 (NC)	0.9456
Scd4	Stearoyl-CoA desaturase 4	1.14.19.1	−1.3 (NC/↓)	**0.002**

*The list assembled from IMPaLA, GeneCards, Brenda and UniProt databases.

**Considerably up- and down-regulated genes are labeled with arrows (↑) and (↓), respectively (if −2≥LFC ≥2 and $p < 0.05$). LFC value of ~1 means no change (NC) in the expression values regardless of *p*-value. If 2 ≥LFC ≥ −2 and $p < 0.05$, ambiguous designations (NC/↑) and (NC/↓) were used.

***p-values of < 0.05 were considered to be statistically significant (in bold).

Table 6.

Changes in expression values of core genes related to the synthesis of odd-chain and branched fatty acids in tarsal plates of *E3wt* and *E3hom* mice.

Gene*	Enzyme*	EC Number*	*E3hom*/*E3wt*, Linear Fold Change**	*p*-value***
Bckdhb	branched chain ketoacid dehydrogenase E1, beta polypeptide	1.2.4.4	21.1 (↑↑)	**4.21E-10**
Pcca	propionyl-Coenzyme A carboxylase, alpha polypeptide	6.4.1.3	3.6 (↑)	**2.46E-05**
Acox2	acyl-Coenzyme A oxidase 2, branched chain	1.17.99.3	2.8 (↑)	**3.66E-06**
Dbt	dihydrolipoamide branched chain transacylase E2	2.3.1.168	2.2 (↑)	**1.63E-05**
Bckdha	branched chain ketoacid dehydrogenase E1, alpha polypeptide	1.2.4.4	1.6 (NC)	0.0055
Bcat2	branched chain aminotransferase 2, mitochondrial	2.6.1.42	1.2 (NC)	0.1267
Bcat1	branched chain aminotransferase 1, cytosolic	2.6.1.42	1.1 (NC)	0.4486
Acads	acyl-Coenzyme A dehydrogenase, short/branched chain	1.3.8.1	1.1 (NC)	0.4417
Bckdk	branched chain ketoacid dehydrogenase kinase	2.7.11.4	−1.0 (NC)	0.879
Acadsb	branched chain ketoacid dehydrogenase E1, beta polypeptide	1.3.8.5	−1.4 (NC)	0.0777

*The list assembled from IMPaLA, GeneCards, Brenda and UniProt databases.

**Considerably up- and down-regulated genes are labeled with arrows (↑) and (↓), respectively (if −2≥LFC ≥2 and $p < 0.05$). Highly up-regulated genes (LFC > 10) are labeled with double arrows (↑↑). LFC value of ~1 means no change (NC) in the expression values regardless of *p*-value. If 2 ≥LFC ≥ −2 and $p < 0.05$, ambiguous designations (NC/↑) and (NC/↓) were used.

***p-values of < 0.05 were considered to be statistically significant (in bold).

Table 7.

Changes in expression values of genes related to inflammation, stress, injury, and wound healing in tarsal plates of *E3wt* and *E3hom* mice.

Gene*	Enzyme/Protein*	EC Number*	*E3hom*/*E3wt*, Linear Fold Change**	*p*-value***
Vnn1	vanin 1	3.5.1.92	4.29 (↑)	**2.66E–06**
Ifi30	interferon gamma inducible protein 30	1.8.-.-	3.1 (↑)	**0.007**
Cd68	CD68 antigen		2.7 (↑)	**0.0021**
Acp5	acid phosphatase 5, tartrate resistant	3.1.3.2	2.4 (↑)	**0.0028**
zc3h12a	zinc finger CCCH type containing 12A		2.11 (↑)	0.0053
Pla2g7	phospholipase A2, group VII (platelet-activating factor acetylhydrolase, plasma)	3.1.1.4(47)	−2.1 (↓)	**0.0006**
Itgb2	integrin beta 2		−2.2 (↓)	**0.0006**
Lipa	lysosomal acid lipase A	3.1.1.13	−2.2 (↓)	**3.39E-05**
Igsf6	immunoglobulin superfamily, member 6		−2.2 (↓)	**0.0053**
col6a3	collagen, type VI, alpha 3		−2.4 (↓)	**7.33E-06**
Msr1	macrophage scavenger receptor 1		−2.5 (↓)	**3.58E-07**
lum	lumican		−2.5 (↓)	**0.0008**
Epas1	endothelial PAS domain protein 1		−2.9 (↓)	**0.0001**
Timp1	tissue inhibitor of metalloproteinase 1		−3.0 (↓)	**1.04E-07**
fcer1g	Fc receptor, IgE, high affinity I, gamma polypeptide		−3 (↓)	**4.31E-06**
tyrobp	TYRO protein tyrosine kinase binding protein		−3.1 (↓)	**1.20E-06**
Cd53	CD53 antigen		−3.2 (↓)	**7.98E-06**
Col3a1	collagen type III alpha 1 chain		−3.2 (↓)	**0.0001**
Col1a2	Collagen type 1 alpha 2 chain		−3.3 (↓)	**2.35E-05**
mmp2	matrix metallopeptidase 2	3.4.24.24	−3.6 (↓)	**9.72E-05**
C3ar1	complement component 3a receptor 1		−3.9 (↓)	**1.28E-06**
Atp6v0d2	ATPase, H+ transporting, lysosomal V0 subunit D2		−5.2 (↓)	**2.19E-08**
Cybb	cytochrome b-245, beta polypeptide		−5.2 (↓)	**1.84E–05**
slamf7	SLAM family member 7		−5.3 (↓)	**1.58E-08**
Spp1	Osteopontin, secreted phosphoprotein 1	3.1.3.-	−6.7 (↓)	**3.68E-07**
Ctss	cathepsin S; cathepsin S (Ctss), transcript variant 1	3.4.22.27	−6.9 (↓)	**3.66E-06**
Defb1	defensin beta 1		−6.97 (↓)	**3.49E-09**
gpnmb	glycoprotein (transmembrane) nmb		−8.2 (↓)	**1.29E-05**
Iqgap2	IQ motif containing GTPase activating protein 2		−8.86 (↓)	**5.54E-08**
Ifi204	interferon gamma inducible protein 30 (*Ifi16* in humans)		−33.0 (↓↓)	**3.44E-10**
Skint3	selection and upkeep of intraepithelial T cells 3		−266.6 (↓↓)	**3.38E-16**

*The list assembled from IMPaLA, GeneCards, Brenda and UniProt databases.

**Considerably up- and down-regulated genes are labeled with arrows (↑) and (↓), respectively (if −2≥LFC ≥2 and $p < 0.05$). Highly down-regulated genes (LFC < −10) are labeled with double arrows (↓↓).

*** *p*-values of < 0.05 were considered to be statistically significant (in bold).